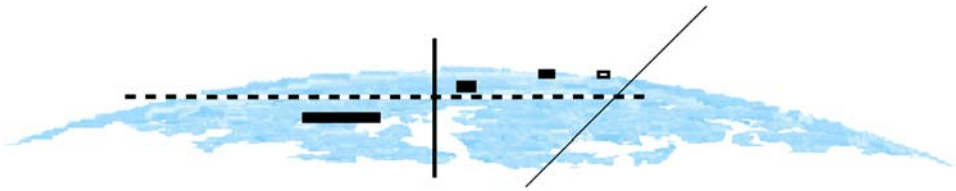

GeoForschungsZentrum Potsdam

STIFTUNG DES ÖFFENTLICHEN RECHTS

Scientific Technical Report

ISSN 1610-0956

MEXAGE
Mexican Aero-Geophysical Experiment
Survey Report

U. Meyer & H. Pflug

GeoForschungsZentrum Potsdam (GFZ)
Department 1 „Geodesy and Remote Sensing“
Section 1.3 ”Gravity Field and Earth Models”
D-14473 Potsdam, Telegrafenberg A17, Germany
umeyer@gfz-potsdam.de, pflug@gfz-potsdam.de

Summary: This report describes the set-up, logistics and results of the MEXAGE (Mexican Aero-Geophysical Survey) survey (Figure 0.1). It gives a short overview about the scientific intentions, detailed documentation of all technical aspects starting from the survey equipment via the aircraft installation to the GPS stations set-up to the experiences in flight. The processing results for the individual profiles are briefly discussed.

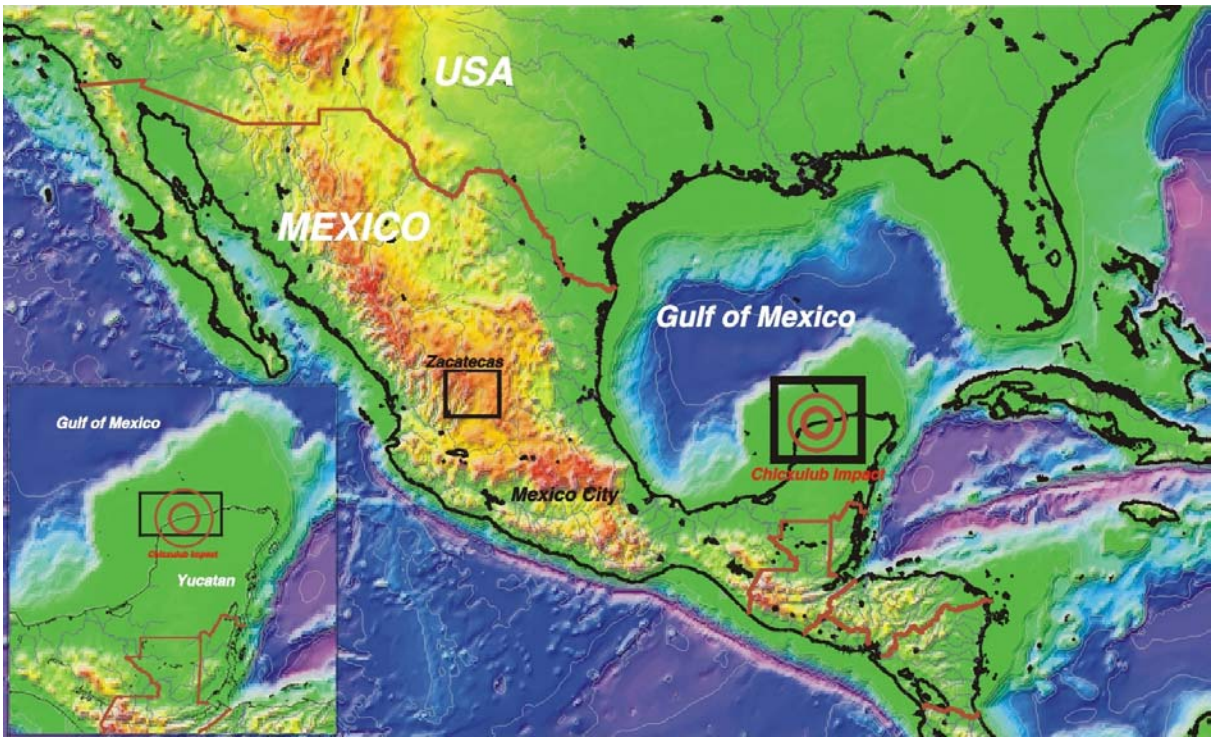

Figure 0.1: Large image: The state of Mexico and the Gulf of Mexico. The black frames indicate the survey areas. Small image in the lower left: The Yucatan peninsula in detail. The red rings indicate the inner and outer radius of the impact crater.

Contents

1 Introduction

Figure 1.1: Views on the town of Puerto Chicxulub, Yucatán, México.

1.1 Motivation

The MEXAGE project was initiated and conducted in co-operation between the Universidad Nacional Autónoma de México (UNAM), hereby the Instituto Geofísica, the Consejo de Recursos Minerales de México (CRM, el Servicio Geologico de México) and the GFZ Potsdam. The goal of the survey was to fly aerogravimetry and aeromagnetometry over the Chicxulub impact structure in the northern part of Yucatán (Figure 1.1) and the southern part of the Gulf of Mexico, using the assistance of the Instituto Geofísica of UNAM and an aircraft of the CRM.

To the present knowledge, the Chicxulub crater was caused by a meteorite impact about 65 million years ago (Campos-Enriquez et al, 1998). It is believed that among other environmental factors this impact was mainly responsible for mass extinction and therefore marks the transition from Cretaceous to Tertiary (K/T-Boundary) (Hildebrand et al., 1998). Although the Chicxulub crater is one of the best preserved impact structures worldwide, it has no significant topographic expression but is buried under Karst and sediment layers (Pope et al., 1996). The northern part of the impact structure is covered by the shallow waters of the southern Gulf of Mexico. It's southernmost part is not accessible for research vessels because of its riffs and shoals close to the coast.

Consequently, a large data gap remained in the most important, central part of the Chicxulub crater. Therefore, this area was mapped during the MEXAGE survey by aero-geophysical means to gather a new and detailed picture of the impact structure. This newly acquired data will be coupled and linked to existing data sets and models. The frame of this study is meant to support further processing beyond this report to compute accurate gravity anomalies and geoid undulations in the survey area, to update and enhance existing 3D-models with the new data and to prove and discuss hypotheses concerning the depth structure and possible Moho-disturbances.

1.2 Existing data

The subsequent paragraphs are meant to document the geophysical and geodetic data that are available beyond the scope of the MEXAGE survey. All reported data so far suffer from bad resolution or sparse data coverage in the southernmost off-shore parts.

1.2.1 MEXICO'97 data

Figure 1.2 shows the best gravimetric data set available at the time, collected, processed and released by the MEXICO'97 geoid project of the United States National Geodetic Survey (US NGS), the Instituto Nacional de Estadistica, Geografia e Informatica (INEGI), and the National Imagery and Mapping Agency (NIMA, later Defense Mapping Agency (DMA), now National Geo-Spatial Intelligence Agency (NGA)). The geoid solution is shown in figure 1.3. For further information please refer to Dr. Dru A. Smith, National Geodetic Survey, NOAA, N/NGS5.

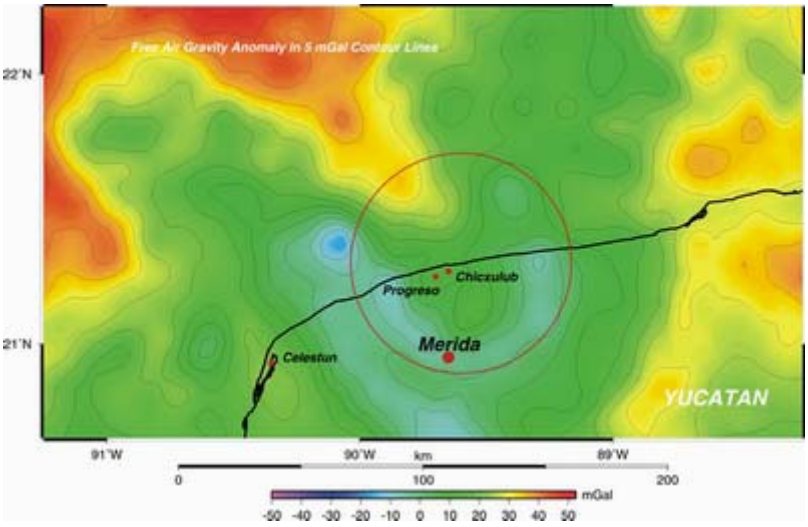

Figure 1.2: Free-air gravity anomaly grid as part of the MEXICO'97 gridded data release.

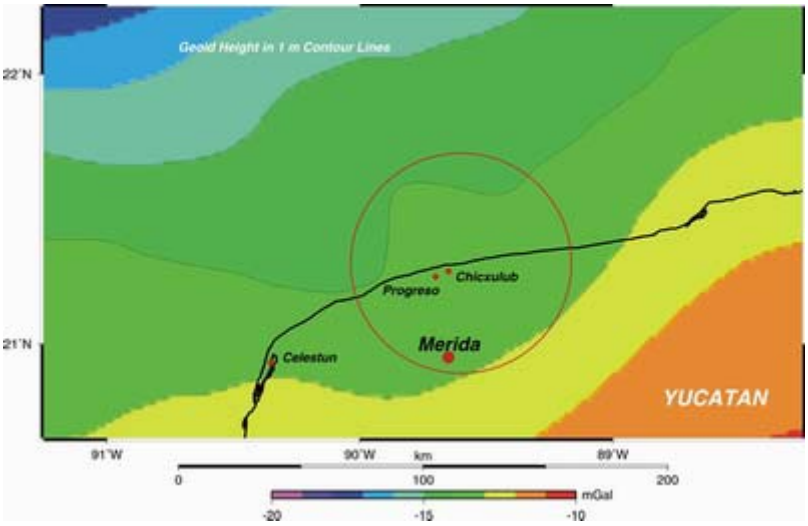

Figure 1.3: Geoid height map derived from the MEXICO'97 grid data. The geoid disturbance by the Chicxulub impact structure is clearly visible.

1.2.2 Seismic data

Two reflection seismic profiles with a total length of 350 km are available through PEMEX (Petróleos Mexicanos), acquired in 1991 about 40 km off the coast of Yucatán. In September / October 1996 another seismic experiment followed, initiated by BIRPS (British Institutions Reflection Profiling Syndicate) and conducted by Geko Prakla, Houston. Within this experiment, parallel to marine reflection seismics (450 to 600 km of profiling) wide-angle observations using OBS-systems (OBS–ocean bottom seismometer) were performed. Additionally, on land the shots from the ship as well as natural earthquakes were observed in prolongation of the marine profiles. A more detailed experiment description and data processing results are given in Morgan et al. (1997). The positions of the profiles are shown in Figure 1.4. It is clearly visible that the marine profiles only touch the outermost parts of the inner crater structure.

1.2.3 Marine gravimetry

In the area of main interest about 16 N-S striking and some crossing profiles are mapped (USGS, 1971, Oregon State University, 1985) with an average distance of about 30 km, up to 30 km close to the coast of Yucatán (Ness, 1991). The positions of the profiles are shown in Figure 1.4 overlaying the free-air anomaly map derived from the described marine gravimetry survey. Please note that the suggested ring structure seen in the free-air anomalies is mostly an interpolation feature and not fully supported by data. The data grid in figure 1.2 is more conservatively computed and does not show a continuation of the ring structure just north of the coastline.

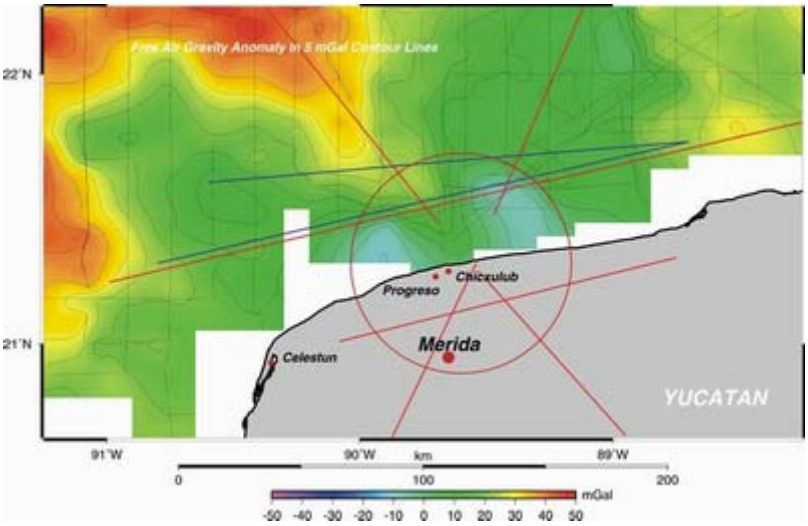

Figure 1.4: Shown is the free air anomaly in mGal computed from the available marine gravimetry data (USGS; Oregon State University; source: BGI, Toulouse). Additionally, the seismic profiles of PEMEX (dark blue) and the BIRPS experiment (red) are indicated.

1.2.4 Terrestrial gravimetry

Onshore, several hundred single point measurements over and around the impact structure are available (Espindola et al., 1995). Unfortunately, this data was not available for our studies. The BGI database holds only 8 gravity stations in the onshore survey area.

1.2.5 Aeromagnetometry

It exists a 1km x 1km data grid computed from an airborne survey conducted by PEMEX (Petróleos Mexicanos) / Goldeneye Explorations Ltd. in 1978 with a line spacing of 6 km and a mean altitude of 450 m, processed and modeled by Pilkington and Hildebrand (2000)

(Figure 1.5). Rebolledo et al. (2003) modelled the central part of the Chicxulub crater using CRM aeromagnetic data from 1997 (2003) (Figure 1.6).

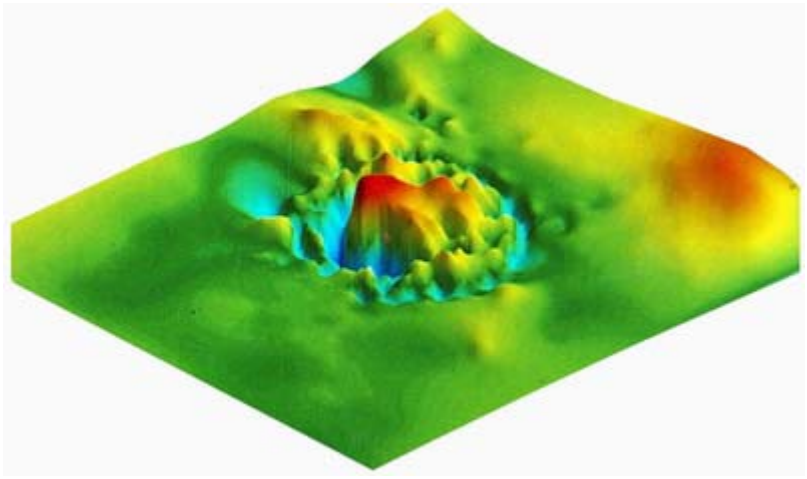

Figure 1.5: Aeromagnetic survey: total magnetic field anomaly map from the PEMEX survey 1978

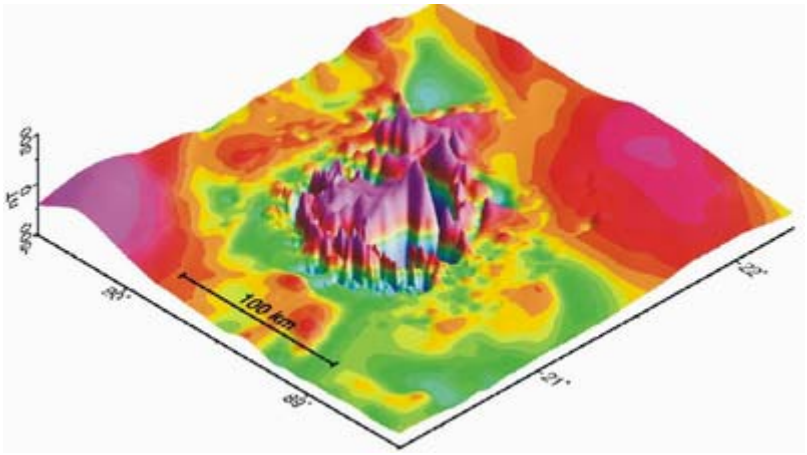

Figure 1.6: Aeromagnetic survey: total magnetic field anomaly map from the CRM survey 1997

1.2.6 Aerogravimetry

PEMEX (Petróleos Mexicanos) conducted an aerogravimetry survey using a Canadian system in the area of Chicxulub and the western mangrove swamps of Yucatán. To our knowledge the data has not been published and inherits several artifacts in its gridded form (Hildebrand et al., 1998). The data is not available.

1.2.7 Satellite altimetry

Due to the lack of large bathymetric roughness and the still coarse resolution in the near coastal area free air gravity derived from satellite altimetry provides only a coarse resolution of the Chicxulub crater. Figure 1.7 shows the compilation version 11.2 of Sandwell and Smith using constrained data only.

A later satellite altimetry derived free-air anomaly compilation of KMS was released in 2001 (Figure 1.8) (Andersen and Knudsen, 1998). The figure shows only a smeared expression of the crater structure. In contrast to the Sandwell and Smith data, the KMS data was fitted to terrestrial NIMA data.

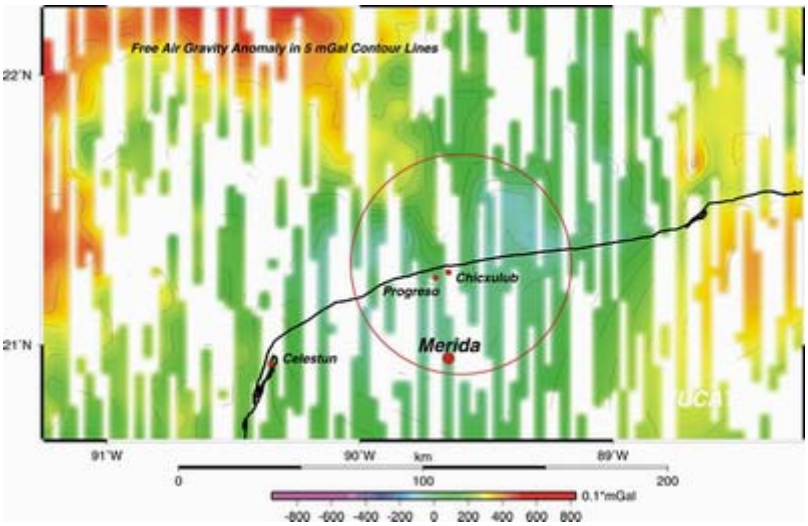

Figure 1.7: Shown is the free air anomaly derived from satellite altimetry after Sandwell and Smith (1997) using constrained data only. The Chicxulub crater north of the coast line is roughly visible.

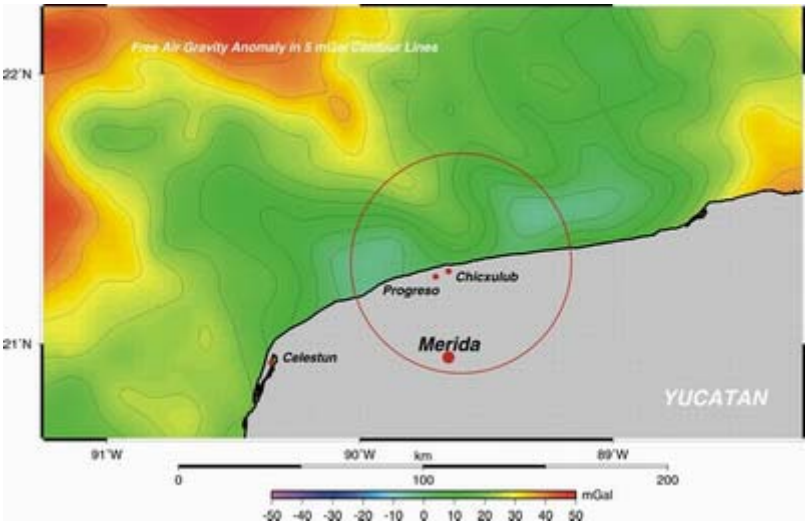

Figure 1.8: Shown is the free air anomaly derived from satellite altimetry after KMS (2001). The resolution in the near coastal areas of Yucatán shows a smeared expression of the impact structure.

1.2.8 Satellite gravimetry

Since the launch of CHAMP (GFZ's CHAllenging Minisatellite Payload Mission) in July 2000 a new epoch in gravity modeling has begun. For the first time the Earth's gravity field can be determined from instrument data of a single satellite. This improvement is due to the well-suited CHAMP instrumentation: High-low GPS measurements guarantee precise homogeneous satellite positioning on a global scale, an onboard accelerometer measures all non-gravitational forces acting on the satellite and a set of star-trackers determine the spacecraft attitude within the inertial reference frame.

GRACE, launched in March 2002 and being a tandem mission, is based for its high-low inter-satellite tracking part on the CHAMP instrumentation with an improved accelerometer. Additionally, the low-low inter-satellite range between the twin satellites is measured very precisely (mm level) with a K-band ranging system. Range variations between the pair of GRACE satellites - only about 220 km apart from each other - are a direct measure of medium to short wavelength features of the Earth's gravity field and therefore the derived

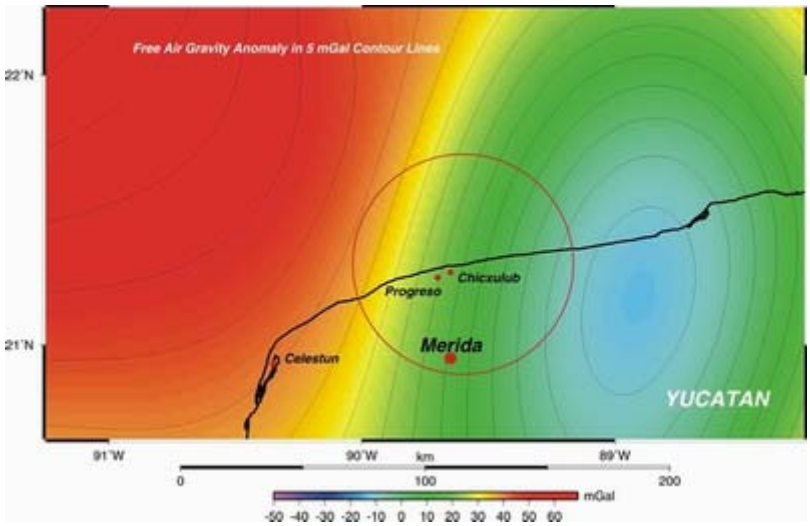

Figure 1.9: Free-air gravity map of GRACE data only (EIGEN-GRACE-02S model).

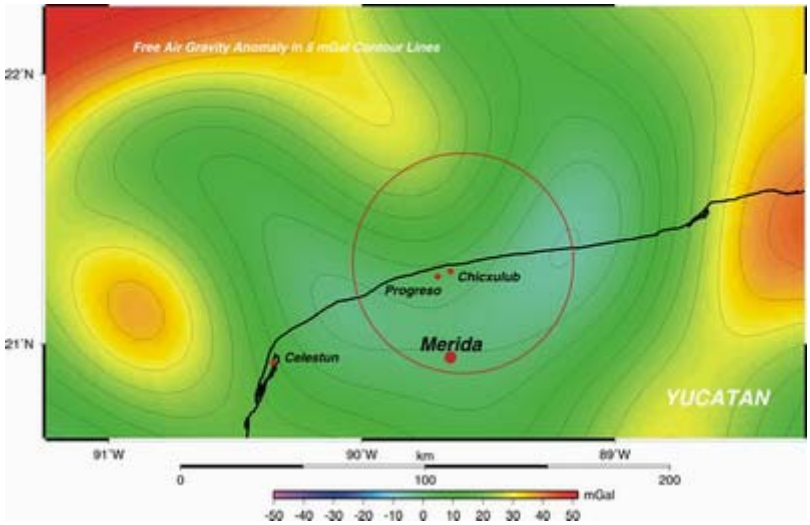

Figure 1.10: Free-air gravity anomaly of GRACE data including surface and altimetry data (EIGEN-GRACE-01C model).

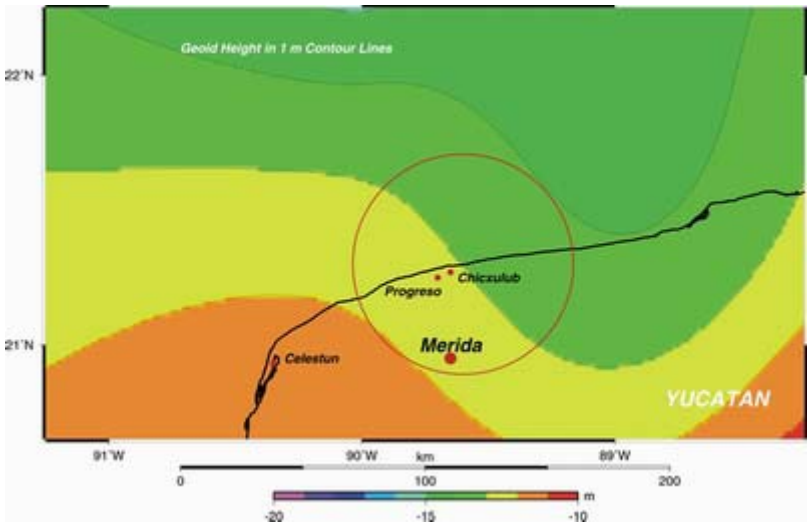

Figure 1.11: Geoid height map derived from GRACE data alone (EIGEN-GRACE-02S model).

EIGEN-GRACE-02S model gives more detail of the Earth's geological features (Schwintzer et al., 2004). Future GRACE gravity models, derived from longer data spans and with further improved processing methods and models, are expected to increase the resolution and accuracy even further. Nevertheless, in the satellite only model EIGEN-GRACE-02S the Chicxulub impact structure is not visible (figure 1.9). It needs the improvement of additional altimetry and terrestrial data to resolve the crater (figure 1.10) (Schwintzer et al., 2004). The same accounts for the geoid representation using GRACE data only (figure 1.11).

1.2.9 Space Radar Topography Mission (SRTM)

The SRTM data over Chicxulub show a subtle, yet unmistakable, topographic indication of the impact crater's outer boundary: a semicircular trough 3 to 5 meters deep and 5 kilometers wide. The impact, centered off Yucatán's coast in the Caribbean, disturbed the subsurface rocks, making them unstable. The rocks were subsequently buried by limestone sediments, which erode easily. The crater rim's instability caused the limestone to fracture along the rim, forming the trough (Figure 1.12).

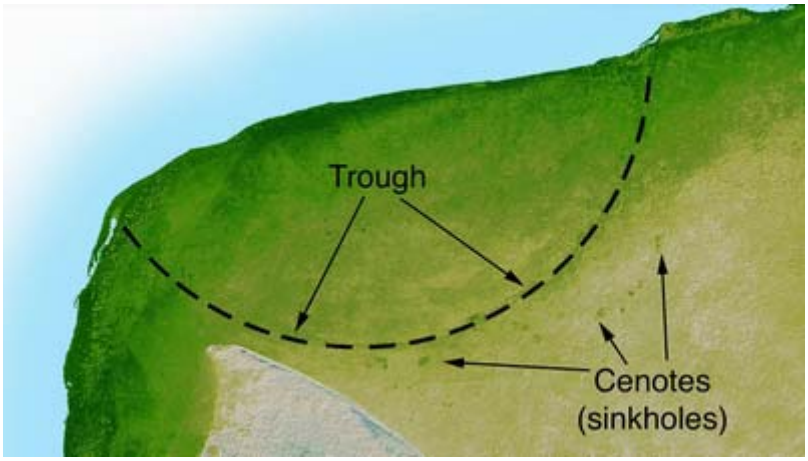

Figure 1.12: As part of a high-resolution mapping database of North America released in March, this picture outlines the 180-kilometer wide Chicxulub crater using radar interferometry from the Space Shuttle Endeavor.

1.3 Existing models and interpretations

Ebbing et al. (2001) present a 3D-model of the central Chicxulub crater on the basis of the so far available, incomplete gravimetric data. Their model shows a crater diameter of about 140 to 160 km with a depth of 1.5 km and a central plateau of 90 km diameter, surrounded by a depression. The central plateau is in good coincidence with the magnetic anomalies and its related model by Pilkington and Hildebrand (2000). Nevertheless, these models were not directly coupled and uniformly computed. In short, the plateau is interpreted as the melt body (long wavelength anomalies) and its load as scattered breccias (short wavelength anomalies).

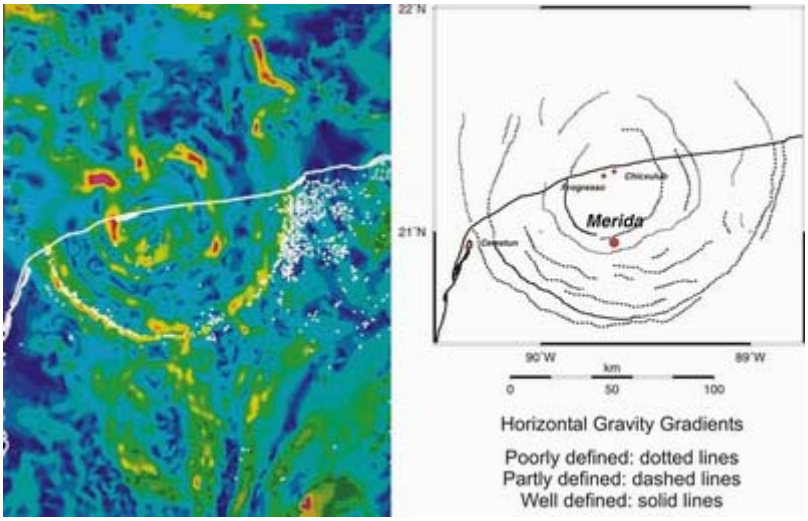

Figure 1.13: Shown are maps of the horizontal gradients of the free air anomalies and derived ring structures of the Chicxulub crater after Hildebrand et al. (1998).

Ebbing et al. (2001) further used their 3D-model to deduce the volume and mass defect for the spatial crater extend, the melt body ($1{,}8 \times 10^4$ km^3) and the sedimentary infill. The derived numbers are – as far as they are comparable – in good accordance with those of Kring (1995). The mass deficit computed by Campos-Enriquez et al. (1998) using Gauss's theorem varies between 6×10^{12} und $1{,}5 \times 10^{13}$ tons. This difference in the mass defect is mainly caused by the integration of a not exactly known gravity variation and ring structure of the crater. A detailed interpretation of the ring structure is given by Hildebrand et al. (1998) (figure 1.13).

The model of Ebbing et al. (2001) (figure 1.14) describes the crater as an undisturbed ring-like structure. The so far available gravity anomalies map the impact zone as a Y-formed structure. These discrepancies from the model (gravity high in the north and gravity low in the south) are discussed but the underlying hypotheses are not integrated and tested in the modeling. Therefore, - among others -the question remains open whether the N-S-striking gravity low around Merida is at least partially impact induced. Boundary conditions for modeling the gravity high in the northwest are given by the analysis of the seismic profile Chicx-B. The detailed knowledge of the crater symmetry and the ejecta distribution leads to important conclusions concerning the impact angle (Schultz and D'Hondt, 1996). Moreover, current analysis of shallow drill cores from Yucatán may give new data and hints to improve the existing 3D-models. The consideration of the newly acquired core data might help to decide whether the gravity low is part of the impact or a rift related structure from the early opening of the Gulf of Mexico (Sharpton et al., 1993).

Furthermore the models of the magnetic anomalies of Pilkington and Hildebrand (2000) are related to a constant magnetic level, not considering an IGRF or other geomagnetic

crustal model. The GFZ continuously updates crustal models from CHAMP satellite data that can be used for a more precise and "sharper" definition of the regional magnetic anomalies, especially when the new and old aeromagnetic data sets are merged.

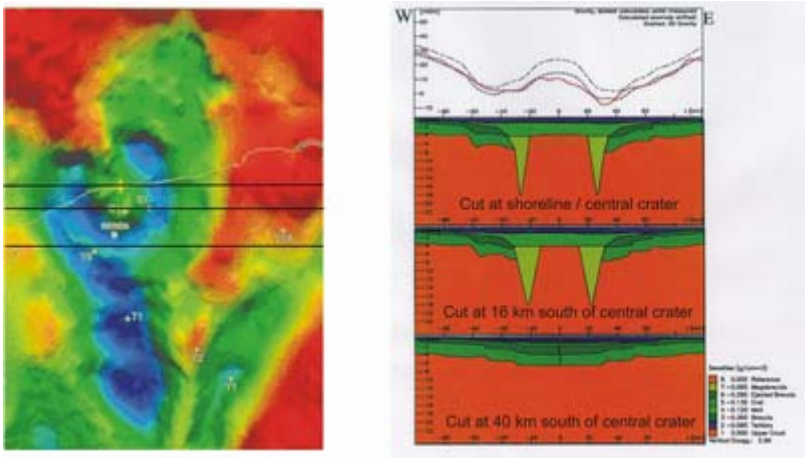

Figure 1.14: Shown are the free air anomaly in the survey area and model after Ebbing et al. (2001). The anomalies are related to E-W profiles over the central crater: red – measured, dotted - 3D-model, dashed – 2D-model.

Morgan et al. (1997) supply moho-depths from seismic data (figure 1.15) that are substantial for most gravimetric models. Comparisons between geoid and isostatic geoid (undisturbed against disturbed moho) over the full extend of northern Yucatán and the adjacent northern shelf gives a clue of how good these depths are determined. If a good regional consistency of the data is achieved, it is possible to test further hypotheses on the basis of the computation of regional isostatic residuals. For the treatment of the isostatic geoid the methods described by Sjöberg (1998) will be implemented into the geoid modeling software. For the treatment of the isostatic residual we propose to use the feature of IGMAS (Götze and Lahmeyer, 1988) and the program described by Jachens et al. (1981) that is exemplarily used in Blakely und Jachens (1990). Such studies have not yet been established on the Chicxulub impact structure.

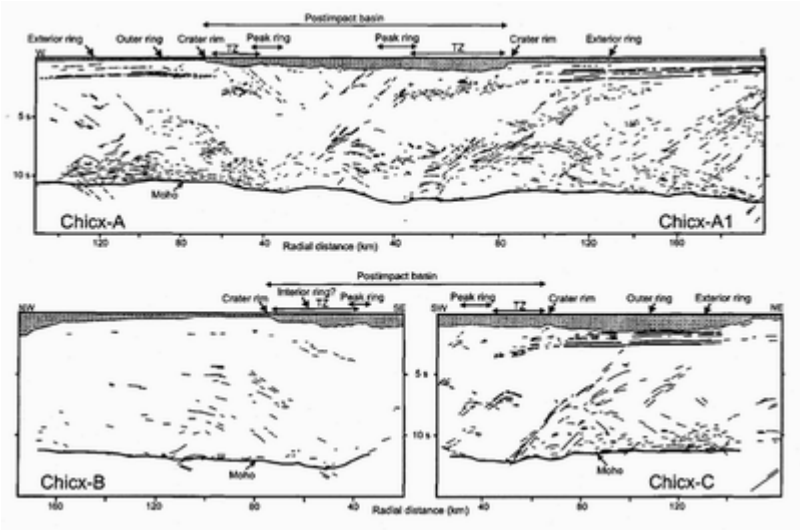

Figure 1.15: Moho-depths from BIRPS-profiles (for location see Figure 1.2) after Morgan and Warner (1999).

For instance, Melosh (1997) describes the possibility that crustal disturbances at the craters rim continue down into the mantle. Would this be the case, these deviations from conventional crustal models (undisturbed moho at the rim) should show up in the free air anomaly and isostatic residual expression. Hildebrand et al. (1998) relate the onshore feature of sinkholes surrounding the central crater (and the missing the any sinkholes in the region of the central crater) to a persisting subsidence of the central crater and its sedimentary infill. After Lopez Ramoz (1975) the subsidence amounts to more than 100 m and therefore might be visible as well in the isostatic residual.

All so far discussed gravimetric models offshore are based on wide spread sampled data with no continuous link to onshore information and therefore display a blurred picture over the northern part of the central crater (Hildebrand, 1998; figure 1.13). Also satellite altimetry derived gravity anomalies contain no more detailed information (Sandwell und Smith, 1997). The newly acquired aerogeophysical data set should enable us not to interpolate but to directly resolve the complex structures of the Chicxulub impact and thus to contribute to an improved 3D-model, also allowing more precise estimations for the volume and mass deficit of the crater as well as for sedimentary infill, breccias and the central melt body.

2 Co-operations and Logistic set-up

2.1 Co-operations

In co-operation with the Universidad Nacional Autónoma de México (UNAM), hereby the Instituto Geofísica and the Consejo de Recursos Minerales de México (CRM) 17 survey flights have been conducted over the area of the Chicxulub impact structure in the time frame from February 8th, 2001 to February 24th, 2001 (see Figure 2.1).

An existent co-operation contract between GFZ and UNAM has been extended to include the conduction of the aerogeophysical survey over the Chicxulub crater. All costs concerning the aerogravimetry system and its installation in an aircraft of the CRM were paid by GFZ, all costs concerning the flight operations by the UNAM. Therefore, the UNAM signed an additional contract with the CRM to enable the usage of a CRM aircraft and their aeromagnetometry equipment including personnel in this project.

The aerogravimetry system of the GFZ was installed in a Britten-Norman Islander (BN202), a small twin-engine aircraft also known as an "island hopper" and so far used for regional aeromagnetic surveys of the CRM. On the CRM's request some test flights were conducted over the highlands south of Zacatecas that were processed apart from the proposed study.

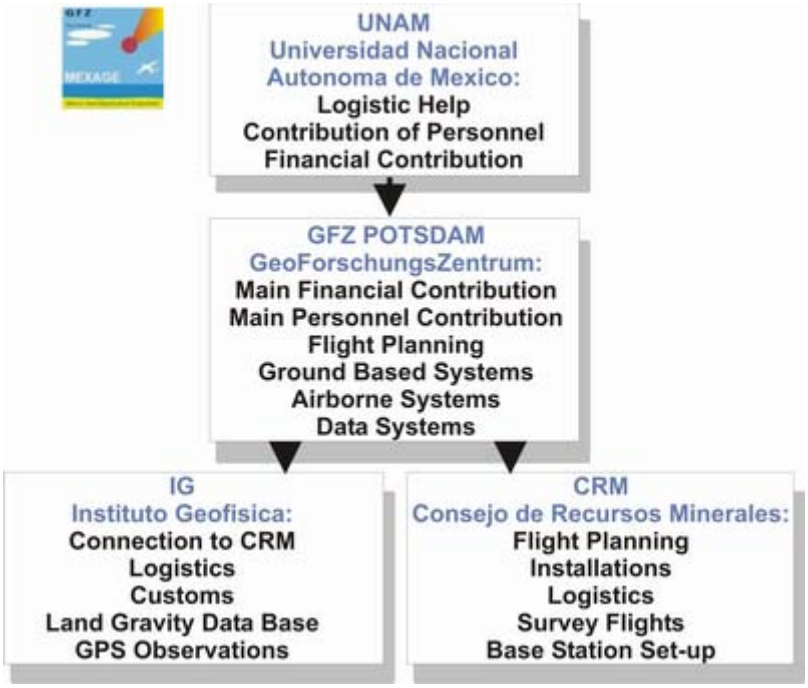

Figure 2.1: GFZ flight profiles over the survey area

All flights in the relevant area of interest were conducted from Merida; GPS-reference stations were installed in Merida, Progreso and Celestun. Since no autopilot system was available, the main flights were performed on E-W striking profiles with a line spacing of 5 km and N-S crossing profiles with a spacing of 30 km. In addition to the simplified navigation for the pilots this pattern offered the most stable flight attitude due to the strong and steady winds from eastern directions over the southern Gulf of Mexico. The chosen flight level was 600 ft over water and 1500 ft over land. The higher flight level over land was imperative due

to close to ground turbulences and is the result of a compromise between the resolution of measurements and flight stability.

Necessary ground based measurements were supported and partly independently conducted by the UNAM team. All flights were undertaken and supported by CRM's aircraft personnel and scientific operators. The magnetic ground base station was part of the CRM's support for the project.

The aircraft installation and first system test flights were done in Pachuca, south of Mexico City. The CRM had rented some hangars there for their research aircraft. Moreover, in Pachuca the headquarters of the CRM are located.

2.2 GPS Stations Zacatecas / Aguascalientes

The CRM requested some test flights in the area between Zacatecas and Aguascalientes, over the Mexican highlands (figure 2.2). The airport used for the survey was located in Zacatecas. The local GPS sites are shown in figures 2.3 and 2.4.

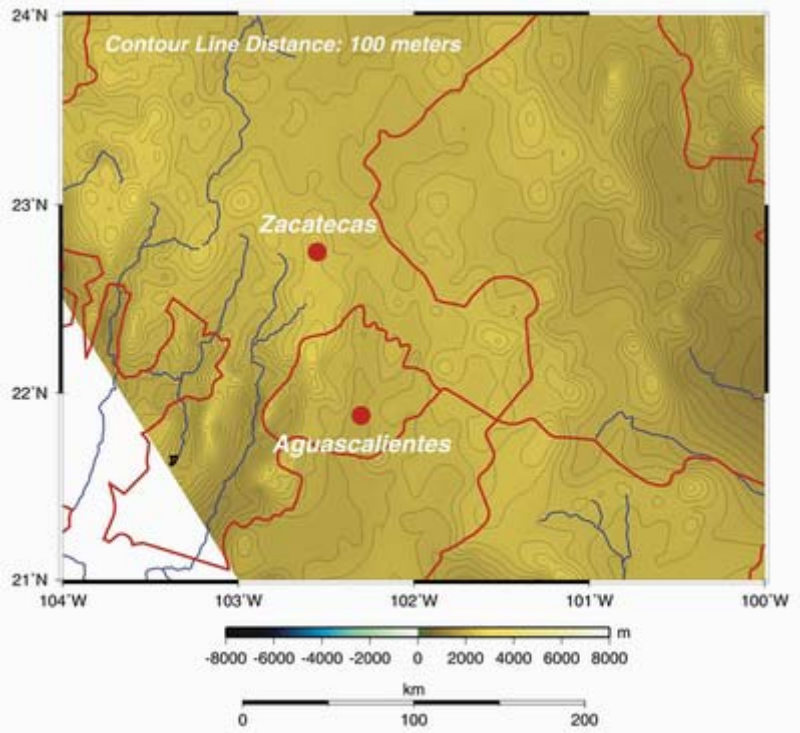

Figure 2.2: Topography of the Mexican highlands including the cities for GPS stations.

Figure 2.3: GPS station on top of side roof on hangar of Zacatecas airport.

Figure 2.4: GPS station on top of roof on a hotel in Aguascalientes.

2.3 GPS Stations Yucatan

The GPS locations for the main part of the survey were located in Merida, the airport used as the base of the campaign (figure 2.6), Celestun and Progreso. The station in Progreso was set up on a daily basis, using two different location (figure 2.6 and 2.7). GPS stations I in Celestun and Merida were permanently installed during the survey time (figure 2.8 and 2.9).

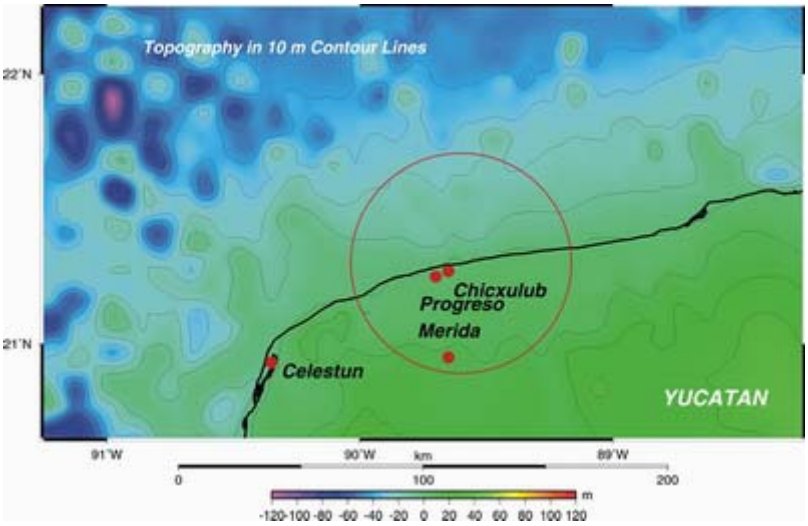

Figure 2.5: Topography and bathymetry on- and offshore Yucatan. GPS stations were set up in Celestun, Progreso and Merida.

Figure 2.6: GPS station in Progreso (first week).

Figure 2.7: GPS station in Progreso (last weeks).

Figure 2.8: GPS station at Merida airport. The GPS antenna was set up behind the FBO sign.

Figure 2.9: GPS station in Celestun, close to the beach.

3 Survey aircraft and crew

3.1 Survey aircraft

The aircraft used for the MEXAGE survey is a Britten-Norman Islander B202 (figure 3.1). This type of aircraft is used all over the world as an island-hopper because of its reliability and stable flight performance. Most of the Britten-Norman Islander aircraft still in service are more than 20 years old. The Britten-Norman Islander of the SAF had a service lifetime of about 26 years. CRM had used it so far only for aeromagnetometry surveys. For the GFZ, it was the first installation of its aerogravimetric survey system in a B202. The scientific instruments were installed by the GFZ team. The major disadvantage was the lack of an autopilot.

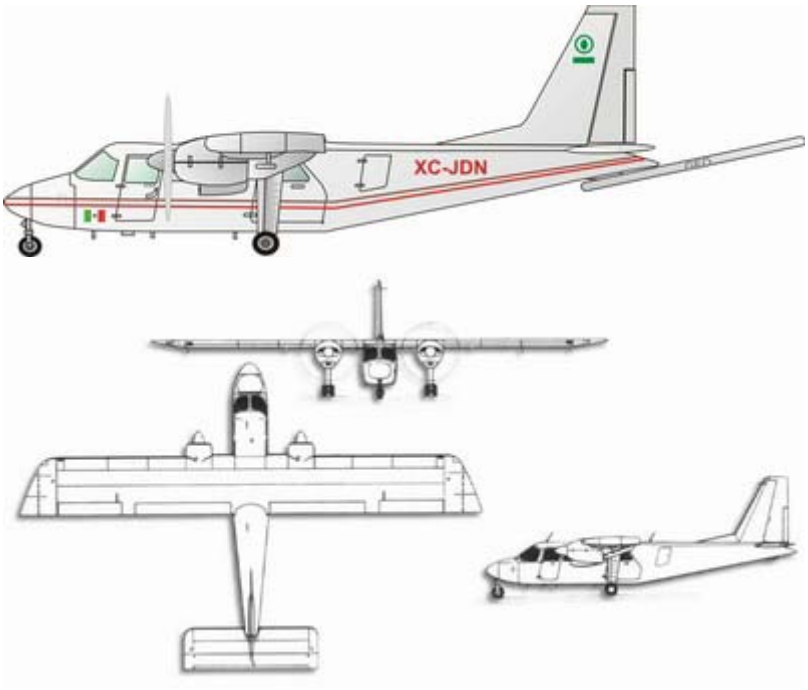

Figure 3.1: Drawings of the de Havilland DHC-6 Twin Otter aircraft of the Servicio Aerofotogramétrico (SAF) in Santiago.

General technical details of the aircraft are given in Table 3.1.

Type:	twin piston engine aircraft
Crew:	2 pilots plus max. 2 scientists with equipment
Ceiling:	13600 ft
Speed:	40 to 142 kts
Weight:	4020 lbs (6600 lbs max. take-off and landing weight)
Load:	2486 lbs (1706 lbs with max. fuel)
Wingspan:	49 ft
Length:	35 ft 8 in (total external)
Height:	14 ft 6 in(external height)
Cabin length:	~ 200 in (internal)
Cabin height:	~ 4 ft (internal)
Cabin width:	~ 45 in (internal)

Table 3.1: Technical details of the de Havilland DHC-6 Twin Otter

The aircraft showed no major technical failures and therefore could be used for all survey flights without delays.

3.2 Aircraft crew

The aircraft crew consisted of members from CRM (for the flights from Pachuca and Zacatecas one pilot, one aircraft technician and three scientist, for the flights from Merida one pilot, one aircraft technician and two scientist), from UNAM (one scientist, for the Zacatecas part two students) and from GFZ (one scientist, one PhD-student, one engineer and one technician).

Figure 3.2: Pachuca / Zacatecas survey team including pilots, aircraft technicians and science crew.

Figure 3.3: Merida survey team including pilots, aircraft technicians and science crew.

4 Aircraft installations

All documentation for the mechanic and electric installation was documented before the survey. This work guaranteed a quick set-up of the instruments on board of the aircraft. The interface between aircraft and scientific instrumentation were mounting plates on the mechanic side and connection to primary ground and aircraft power on the electric side. Some more work was required for the installation of the laser altimeter. Figure 4.1 shows the work on the aircraft and part of the installation. Figure 4.2 shows a schematic overview of the aircraft installation.

Figure 4.1: left: weight and balance inspection; right: LaCoste & Romberg gravity meter, in the rear the cockpit.

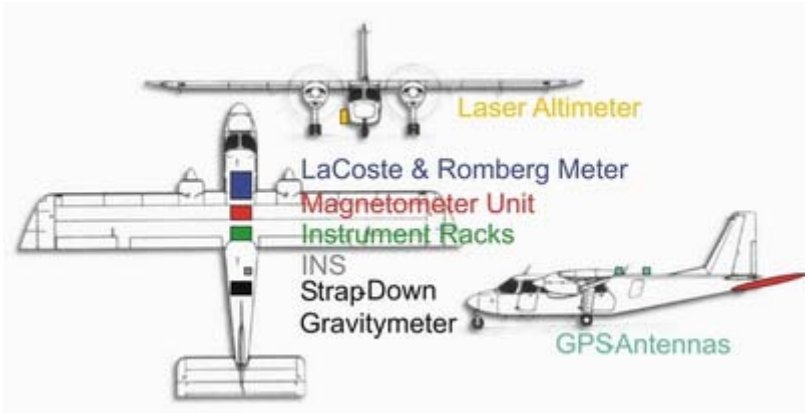

Figure 4.2: Mechanic installation of the ANGEL system in the Britten-Norman Islander B202.

The instruments had to be installed in way that the weight and balance of the aircraft was still in the allowed frame. An overview about the installed instruments and their weights are given in Table 4.1. The electric power consumption of the main instruments is given in Table 4.2.

Instrument *Instrument*	Gewicht *Weight* [kg]
Grundplatte Instrumentengestell / Bottom Plate Intrument Rack	?
Instrumentengestell ohne Bestückung / *Instrument Rack without Equipment*	12.0
IGI INS-Console / IGI INS-Console	7.0
LaCosta Romberg PC / LaCosta Romberg PC	20.5
GPS PC Console 19"-Einschub / GPS PC Console 19" Unit	15.0
Windows PC Console 19"-Einschub / Windows PC Console 19" Unit	8.0
Meinberg Trigger 19"-Einschub / Meinberg Trigger 19" Unit	10.5
PC- Umschalter / PC-Switch	1.0
Stromverteilung Schaltkasten / *Power Distribution Switch Board*	9.0
Grundplatte Operatorgestell / Bottom Plate Operator Rack	?
Operatorgestell ohne Bestückung / Operator Rack without Equitment	4.0
Inverter / Inverter	8.5
Bildschirm / Monitor	1.0
Tastatur und Maus / keyboard and mousepanel	0.5
Grundplatte Laser-Altimeter / Bottom Plate Laser-Altimeter	?
Laser-Altimeter Sensor / Laser-Altimeter Sensor	2.0
Netzteil / Power Unit	2.0
Magnetotmeter – Console / Magnetometer – Console	5.0
Magnetotmeter – Sensor / Magnetometer - Sensor	1.5
Grundplatte IGI System / Bottom Plate IGI System	?
IGI INS E-Box / *IGI INS E-Box*	8.0
IGI INS Sensor / IGI INS Sensor	2.0
Grundplatte SAGS 2.2 / Bottom Plate SAGS 2.2	
SAGS 2.2 Sensor + Plattform/ *SAGS-2.2 Sensor+ Rack*	52.0
Grundplatte Gravimeter / Bottom Plate Gravimeter	?
Netzteil UPS / Power Unit UPS	30.0
LaCosta Romberg Gravimeter / LaCost Romberg Gravimeter	50.0

Table 4.1: Installed instruments and weight.

Elektrischer Verbraucher **Electrical Unit**	**Leitstungsaufnahme** **Power Consumption**
Laseraltimeter Z-LAS-01	10 Watts @ 28 VDC
SAGS-2 Sensor Z-SAG-01 Meinberg Clock Z-MBC-01	70 Watts @ 28 VDC 10 Watts @ 220 VAC
GPS PC Z-GPS-PC-01 WIN PC Z-WIN-PC-01	150 Watts @ 220 VAC 150 Watts @ 220 VAC
Magnetometer Z-MAG-01	50 Watts @ 220 VAC
IGI-Console Z-IGI-01 IGI-IMU / Sensor Z-IGI-02 Ashtech GPS Rx Z-ASH-01	50 Watts @ 28 VDC 300 Watts @ 28 VDC 7.5 Watts @ 28 VDC
S124 Gravitymeter Z-LLC-01	300 Watts @ 220 VDC

Table 4.2: Main instruments and their power consumption.

5 Aircraft equipment

5.1 LaCoste & Romberg S124b gravity meter system

The LaCoste & Romberg air/sea gravity meter Model S124b (Figure 5.1) consists of a highly damped, spring type gravity sensor mounted on a gyro stabilized platform with associated electronics to obtain gravity readings. The original theory behind the LaCoste & Romberg Air/Sea gravity meter is given in LaCoste et al. [1967]. Technical details about the instrument are given in Tables 5.1 and 5.2.

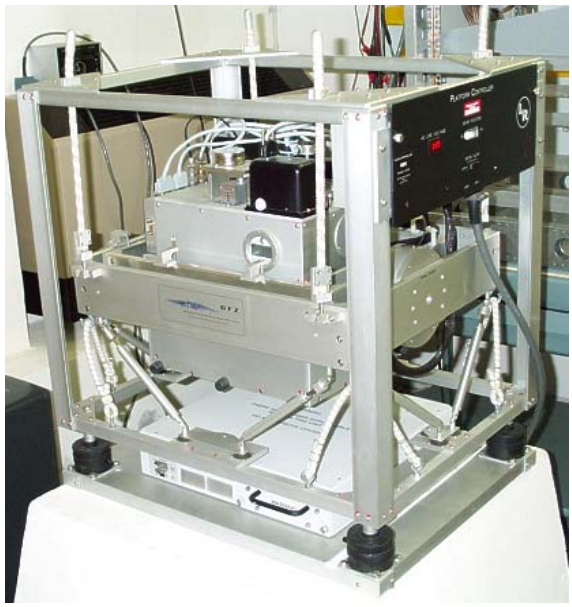

Figure 5.1: LaCoste & Romberg S124b gravity meter in GFZ laboratory

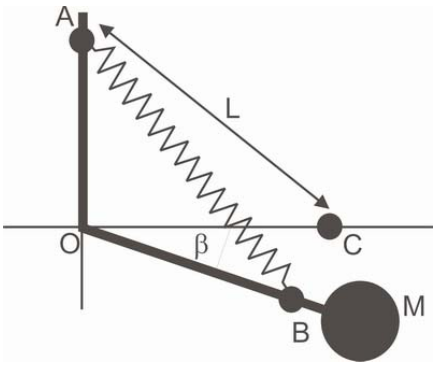

Figure 5.2: Simplified principle of a zero-length suspension system: The mass M is attached to the moveable beam OB that is free to rotate about O. The beam is supported by a zero-length spring attached at the points A and B. In practice, the beams total travel distance between top stop and bottom stop is about some mm in the Model S meter.

The Model S sensor incorporates a hinged beam supported by a zero-length spring (a zero-length spring is a spring whose equilibrium length with a test mass attached is zero, see Figure 5.2). The damping of the large vertical accelerations due to the aircraft's motion is achieved through the use of internal air dampers. Nevertheless, the vertical accelerations of the aircraft makes it impossible to keep the beam constantly nulled. Therefore, it is necessary to read the gravity sensor when the beam is in motion. A mathematical analysis of the spring

type gravity sensor shows that this is possible through the observations of: the beam position, the beam velocity and the beam acceleration at any given time. If the beam motion is highly damped, the beam acceleration term can be neglected. If the gravity sensor has a very high sensitivity over a high range, the beam position can be neglected as well. The LaCoste & Romberg S-meter fulfils both requirements. Accordingly, it can be read without nulling it via the measurement of the beam position parallel to the adjusted spring tension.

Utilizing the zero-length spring principle in a particular geometry results in a vertical suspension that can have infinite periods [LaCoste et al., 1988]. When the period is infinite and the torque exerted by the spring tension exactly balances the torque exerted by gravity, the beam will remain stationary at any position. When this position is achieved, the smallest change in gravity will cause the beam to rotate to one stop or the other. Thus, infinite period corresponds to infinite sensitivity [Valliant et al., 1992]. If the period is less than infinite and the beam is displaced from its equilibrium position, a restoring torque will return it back to the equilibrium position – this is the case for land gravity meters.

So finally, for the Model S meter the basic equation to gain the relative gravity at a given time and thus at a given location is:

$$dg = S \times M = \text{Spring Tension} + k \times \text{Beam Velocity} + \text{Cross Coupling Errors}.$$

Here, k is a constant depending on the adjustment of the physical damping which is mainly dependant on the quality of the air dampers implemented in the system (see Figure 5.3). M is the actual measurement in scale units; S is the scale factor to convert the readings into mGal. Of course in our case dg only represents a relative measurement meaning only the changes in the gravity field are detected.

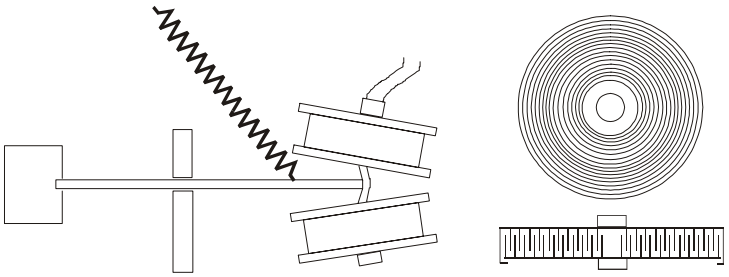

Figure 5.3: Schematic sketch on beam damping (right end of beam with hose for air pump) and box for capacitive beam position measurement (left end of beam) plus top and side cut view of an air damper.

For best performance and accuracy of the airborne gravity measurements it is mandatory to keep the platform that holds the gravity meter system as close to horizontal level as possible. For this task for each of the two horizontal axes an accelerometer and a gyro is implemented. The accelerometer itself is being manually controlled and leveled when the gravity meter is in an undisturbed environment. The accelerometer then is being nulled with the help of a precise water level on top of the platform. The output signal of the accelerometer is linear with the tilt angle of the platform and has a maximum range of about 16°. The accelerometer signal is sent to the gyro processor meaning the signal is appropriately shaped for gyro input. The gyro itself only measures the angular rates of the platform but has no information of its own about the spatial orientation. Therefore, the accelerometer input is needed. The combined signals are filtered and sent to the servomotor to correct actual deviations of the platform from the horizontal (see Figure 5.4). The reaction time of this negative feedback loop is close to immediate but it has a limited “memory” due to the gyro drift. The memory time used with the filter is about 5 minutes for airborne application and 11

minutes for ship operations. On the LaCoste & Romberg S124b platform optical gyros are used for attitude control. They do not need any heating as mechanic gyros and have excellent control about rapid angular changes.

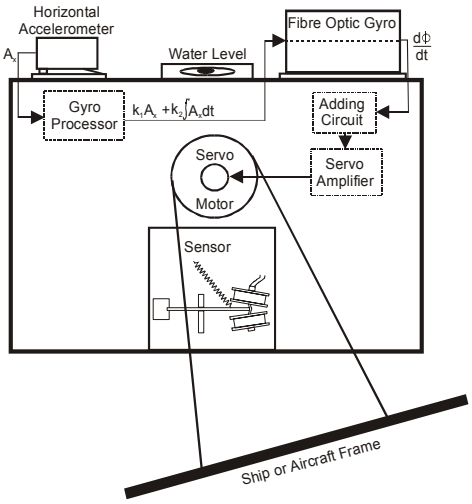

Figure 5.4: Schematic sketch of the platform horizontal leveling in one axis

Platform physical size:	55 cm (22”) W x 70 cm (27”) D x 64 cm (25”) H
Platform weight with sensor:	79 kg (175 lbs.)
Center of gravity height:	28 cm (15”)
Driver / Computer unit size:	46.5 cm (19”) W x 48 cm (18.9”) D x 27 cm (10.6”) H
Driver / Computer unit weight:	21 kg (46 lbs.)
Keyboard unit size:	46.5 cm (19 “) W x 44 cm (17.3”) D x 4.5 cm (2”) H
Keyboard unit weight:	7 kg (15.5 lbs.)
UPS physical size:	43.3 cm (17”) W x 41 cm (16”) D x 9 cm (4”) H
UPS weight:	19 kg (42 lbs.)
Operating temperature:	0°C to 40°C (32°F to 104° F)
Storage temperature:	-30°C to 50°C (-22° F to 122° F)
Power requirements:	300 Watts @ 115/230 VAC or ~ 1.5 A @ 230VAC

Table 5.1: Physical properties of the LaCoste & Romberg S124b gravity meter

Range:	12,000 mGal
Drift:	3.0 mGal per month or less
Temperature set point:	49° C
k-Factor (internally, static beam):	1.37
k-Factor (externally, dynamic beam):	39.0
Scale-factor (spring tension):	1.014
Stabilized platform specification	
Platform pitch (mechanical):	± 25 degrees
Platform roll (mechanical):	± 25 degrees
Platform pitch (accelerometer range):	± 16 degrees
Platform roll (accelerometer range):	± 16 degrees
Platform period:	4 minutes
Platform damping:	0.707 of critical period
Control systems specifications	
Recording rate:	1Hz plus 10Hz for beam positions (AIRSEA 3.1)
Serial output:	RS-232
Additional output:	3 analogue channels (±10V)
Gravity systems specification:	
Accuracy in laboratory:	50000 mGal horizontal acceleration (± 0.25 mGal) 100,000 mGal horizontal acceleration (± 0.50 mGal) 100,000 mGal vertical acceleration (± 0.25 mGal)

Table 5.2: Performance parameters of the LaCoste & Romberg S124b gravity meter

5.2 SAGS 2.2 strap-down gravity meter system

The strap-down system described in the following section is owned and developed by the Bayerische Akademie der Wissenschaften in München (BADW). Responsible for the design of the instrument and the research on this topic at the Bayerische Kommission für Internationale Erdmessung (BEK, within BADW) is Dr. Gerd Boedecker.

The strap-down concept offers some important advantages when compared to conventional airborne gravity meters as the LaCoste & Romberg S124b: a potentially higher spatial resolution, an improved and simplified handling, significantly less volume and weight plus the potential to gain gravity vector observations. Other strap-down system developers in the field of aerogravimetry use off-the-shelf inertial navigation systems. These systems suffer from the handicap that they are optimized only to get the navigation and attitude solution precisely but not gravity. They are mostly not temperature controlled, therefore then have high drift rates and generally allow only limited access to the signal processing. Thus, an independent solution from INS packages was strived for. Within SAGS-2.2 (Figure 5.5), Q-Flex accelerometers have been utilized. These sensors still have the best potential for gravity observations and are used as industry reference for acceleration measurements of all kinds. The integral Q-Flex electronics develops an acceleration-proportional output current providing both static and dynamic acceleration measurement. Through the use of a customer supplied output load resistor, appropriately scaled for the acceleration range of the application, the output current can be converted into a voltage. The QA-3000 includes a current-output and an internal temperature sensor. Through the use of a temperature-compensating algorithm bias, scale factor and axis misalignment performance is dramatically improved.

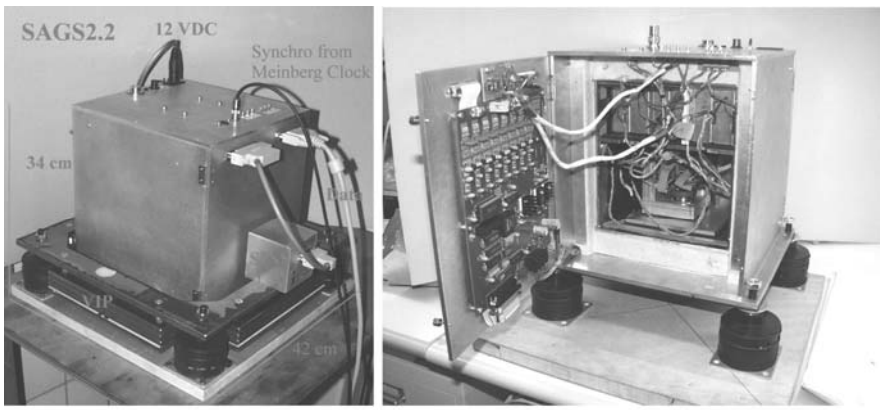

Figure 5.5: SAGS 2.2 in the laboratory of BADW/BEK.

To reduce temperature and electromagnetic noise effects on the Q-Flex sensors special shields were tested and implemented in the SAGS housing. Additionally, a vibration-damping platform to hold the housing was constructed. The SAGS control and data acquisition system was individually developed for this purpose running on a laptop using a MatLab environment.

In detail, SAGS-2.2 implements 3 Q-Flex® Quartz Accelerometer 3000 (QA-3000) within an airborne strap-down system to measure 3D accelerations resulting from gravity and kinematics (see Figure 5.6). Primary applications of QA-3000 include spacecraft navigation and control systems. The QA-3000 features an etched quartz flexure seismic system. The proof mass is etched from a single piece of quartz to form an outer, stationary mounting ring and an inner pendulous disk The disk is connected to the outer ring by two thin flexures or "hinges". These flexures tightly constrain the proof mass and allow rotation only about the hinge axis. The amorphous quartz makes an ideal material from which to form proof mass and flexures, which are essentially perfectly elastic. There is no energy lost in their bending. The

dimensional stability of the material also guarantees unchanging proof mass parameters as size and mass. It provides excellent bias, scale factor, and axis alignment stability. The Q-Flex accelerometer combines advantages of fused quartz with solid-state servo electronics. Acceleration along the sensitive axis creates a force on the proof mass pendulum, displacing it slightly, causing a signal in a capacitive null detector. In response to this signal a servo circuit sends a current through coils attached to the proof mass. The current in these coils, moving through a permanent magnetic field mechanically restores the proof mass to the null or balanced position. The current required to re-balance the proof mass is proportional to the input acceleration. The basic formula for the accelerometer output as a function of the acceleration input is: Output = Scale Factor x (Acceleration along input axis + Bias).

Please note that the scale factor and the bias depend also on temperature, axis misalignment and vibration.

The minimum configuration for strap-down airborne gravimetry systems would be one single accelerometer installed to measure in the approximate vertical component only. The next step to upgrade the system would be to add two tilt meters for the horizontal components. SAGS-2.2 holds the maximum configuration, three Q-Flex accelerometers in an orthogonal system with the best sensor mounted in the vertical component. In an aircraft environment vibrations easily have much larger amplitudes than the gravity signal that is to be determined. They are comparable in amplitude to the aircraft kinematic induced acceleration with only a small frequency gap in between. The SAGS principle of measurement (meaning accelerometer reference, attitude and position reference have a fixed relation) does not allow high damping ranges (below 5 mm). It is still a difficult task to design an optimized vibration-damping platform that suits a range of different aircraft. Three different acceleration signal sources merged have to be processed by SAGS: vibration, aircraft kinematics and the gravity field. As discussed above, vibrations are physically damped by the platform design. The lasting signal is measured by the Q-Flex accelerometers and analogue-filtered. The filtered signal can either be digitized by a frequency counter or by an analogue-to-digital converter. The derived signal on each way now can be filtered digitally and reduced by the accelerations computed from the GPS-signal from aircraft antennas.

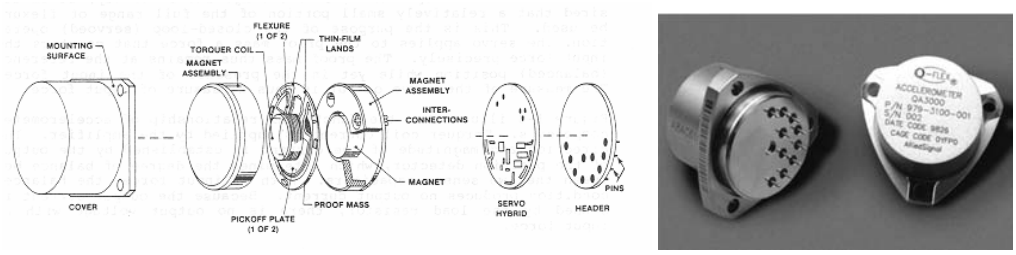

Figure 5.6: Q-Flex accelerometer

Sensor unit physical size:	42 cm (16.5”) W x 42 cm (16.5”) D x 34 cm (13.4”) H
Sensor unit weight:	49.5 kg (109 lbs.) (including SINS & VIP)
Sensor power requirements:	60 Watts @ 12 VDC (initial heating) 15 Watts @ 12 VDC (standard operation)
Meinberg clock physical size:	24 cm (9.5”) W x 36 cm (14.2”) D x 14 cm (5.5”) H
Meinberg clock weight:	4.5 kg (9.9 lbs.)
Clock power requirements:	less than 10 Watts @ 12 VDC or 220 VAC
Data logger – notebook:	Type Kontron / Panasonic CF25 or
Data logger physical size:	30 cm (12") W x 30 cm (12") D x 30 cm (12") H
Data logger weight:	4 kg (8.8 lbs.)
Data logger power requirements:	max. 40 Watts @ 220 VAC

Table 5.3: Physical properties of the SAGS 2.2 strap-down gravity meter system

5.3 IGI inertial navigation system CAE-10-01

The standard system from IGI is a guidance, positioning and management system for aerial survey missions named CCNS4. A special version named CAE-10-01 was adapted to GFZ requirements. The main task of the system is not the flight management but the attitude measurement of the aircraft. Thus, most flight control options were omitted in favor of best control over the raw data. The basic system consists of the central computer unit that handles the data flow, acquisition and visualization. The CAE-10-01 can either be used as a sub-unit of the CCNS4 system with status reports displayed on the CCNS4 information pages or as a stand-alone data acquisition unit. For all airborne missions of the GFZ so far the system was operated in the later mode. This special version CAE-10-01 can be used to control either remote sensing systems or just be taken for aircraft attitude measurements. Together with the AEROcontrol system, based on DGPS and information from an inertial measurement unit (IMU) - it allows real time and post processing of sensor or aircraft frame positions for given instants. The system allows the determination of the elements of exterior orientation (ϕ, ω, κ and x/y/z). Heading information with accuracy of 1/10° and pitch as well as roll information are being furnished with an accuracy of 1/100°.

The principal navigation sensors of the AEROcontrol system are a 12 channel parallel L1/L2 RX GPS receiver (Novatel OEM4) on 1 Hz and a dry tuned gyro with a separate sensor head (modified LITEF LCR 88) on 50 Hz (Figure 5.7). The data output is the system time, the angel increments and the velocity increments both in the x-, y-, z-axes with 50 Hz. Additionally, the system time, the GPS week second and 5 optional channels are recorded with 1 Hz. This IMU and optional sensor data is stored parallel with the Ashtech GPS data on a portable flash disk. Events are time stamped and marked in an extra data channel (waypoints, power settings, etc.). The data can be post-processed using the IGI AEROoffice software – having computed the kinematic DGPS positions from the Novatel OEM4 GPS receiver first. Technical details are given in Table 5.4.

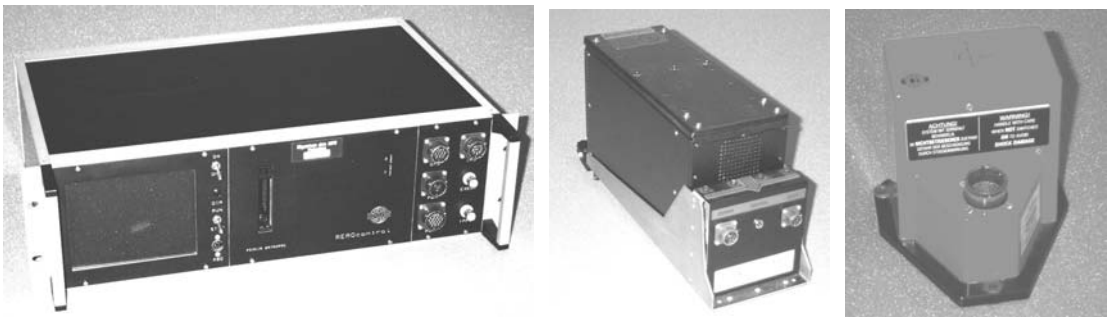

Figure 5.7: IGI inertial navigation system console, electronics box and sensor head

IMU sensor unit physical size:	20 cm (7,9”) W x 20 cm (7,9”) D x 25 cm (9,8”) H
IMU sensor unit weight:	49.5 kg (109 lbs.) (without cable)
IMU E-box unit physical size:	20 cm (7,9”) W x 35 cm (13,8”) D x 25 cm (9,8”) H
IMU E-box unit weight:	49.5 kg (109 lbs.) (without cables)
IMU E-box power requirements:	60 Watts @ 12 VDC (initial heating) 15 Watts @ 12 VDC (standard operation)
CAE-10-01 unit physical size:	48,3 cm (19,0”) W x 36 cm (14.2”) D x 18 cm (7,1”) H
CAE-10-01 unit weight:	4.5 kg (9.9 lbs.) (without cables)
CAE-10-01 power requirements:	less than 10 Watts @ 12 VDC or 220 VAC

Table 5.4: Physical properties of the IGI inertial navigation system.

5.4 GPS receivers

5.4.1 Ashtech Receiver Z-Surveyor

5.4.1.1 Standard Features

- 12 channel all-in-view operation
- Full wavelength carrier on L1 and L2
- Z-Tracking and Multipath Mitigation
- Real-time kinematic for cm-accuracy (rover and base mode)
- Dual-frequency smoothing for improved code differential
- Removable PCMCIA memory card slot
- Internal battery slot for 4.5 hours operation
- Selectable update rate from 1 to 5 Hz (10 Hz optional)
- Real-time data output on NMEA 0183 output
- 1 PPS timing signal output
- Remote monitoring
- Session programming
- External power input
- 4 RS-232 ports (115200 baud max.)

Static, Rapid Static Survey:	5 mm + 1 ppm 2d-rms
Postprocessed Kinematic Survey:	1 cm + 1 ppm 2d-rms
Real-time Differential Position:	< 1 m 2d-rms
Real-time Z Kinematic Position:	moving: horizontal: 3 cm + 2 ppm
	vertical: 5 cm + 2 ppm
	static: horizontal: 1 cm + 2 ppm
	vertical: 2 cm + 2 ppm
Static Occupation Time:	2 sec
Azimuth:	0.15 + 1.5 / baseline in km (arcsec)
RTK on-the-fly initialization:	> 99.9% reliability
RTK initialization time:	< 30 secs following the acquisition of 8 or more satellites
RTK baseline recommendation:	< 10 km
RTK maximum baseline:	< 40 km

Accuracies assume a minimum of 5 satellites at good quality.

Table 5.5: Performance Specifications

Type:	ATA Type II PCMCIA Memory Card
Temperature Range:	-40°C to +85°C
Typical number of epochs:	4500 per 2 Mb @ 8 satellites, 20 secs data rate

Table 5-6: PC-Card Specifications

5.4.1.2. Casing, Connections and Power Supply

Figure 5.8: Ashtech Z-Surveyor Full Front and Rear Side View

The Ashtech Z-Surveyor is connected to the 12 VDC power output of the IGI-AEROControl 19" rack unit.

5.4.1.3. Ashtech Flight Antenna

Figure 5.9: Top and Bottom View of Ashtech Flight Antenna (Scale in cm)

5.4.1.4 GPS Antenna and Antenna Connection

The Ashtech Z-Surveyor is connected to a flat-line antenna with an integral LNA via a standard TNC-type female receptible wired for connection via 50-ohm coaxial cabling. The connector shell is connected to the Z-Surveyor ground. The TNC-type connector center pin provides +5 VDC (to power the LNA) and accepts 1227 and 1575.42 MHz RF input from the antenna. The RF and DC signals share the same path. The current for the GPS antenna connector is limited to 150 mA out of the center conductor. It is short circuit protected. If using a splitter or other RF network, use an inner DC block suitable for 1 – 2 GHz , 50-ohm. Maximum voltage back to the Z-Surveyor cannot exceed 15V.
The antenna type is AT2775-17W-TNCF-000-05-40-NM (AeroAntenna, 5 Volts, 40 dB linear amplification, female TNC connector on antenna) with TSO-C129 for airborne usage.

5.4.2 Trimble Receiver

5.4.2.1 Standard Features

- Super-Trak™ signal processing technology
- RTCM Version 2 input
- Event marker input
- 1 PPS output
- NMEA-0183 output
- Internal memory
- Fully functional, integrated control panel

Static Survey Modes:	Quick-start, Planned survey, Auto-timed survey, Static survey, Fast Static survey
Accuracy:	Horizontal: ±5 mm + 0.5 ppm Vertical: ±5 mm + 1 ppm Azimuth: ±1 arc second + 5 / baseline in km
Kinematic Survey Performance (Postprocessed) Modes:	Continuous, Stop & Go
Accuracy:	Horizontal: ±1 cm + 1 ppm Vertical: ±2 cm + 1 ppm
Occupation:	Continuous: 1 measurement Stop & go: 2 epochs (min.) with 5 satellites
Fastest Continuous Data Rate:	2Hz
Real-time Survey Modes:	Real-time Kinematic (RTK), Real-time Differential (DGPS)
Real-time DGPS accuracy:	0.2 m + 1 ppm RMS
RTK Accuracy:	Horizontal: ±1 cm + 1 ppm Vertical: ±2 cm + 1 ppm
Range:	Range varies depending on radios used, local terrain and operating conditions. Multiple radio repeaters may be used to extend range, depending on type used.
Initialization:	Mode: Automatic while stationary Automatic while moving on the fly (OTF) (optional) Time: < 1 min. (typical) < 10 sec. (typical for known point or RTK initialiser). Reliability >99.9%

Table 5.7: Performance Specifications

Performance criteria are a function of the number of satellites visible, occupation time, observation conditions, obstructions, baseline length and environmental effects, and are based on favorable atmospheric conditions. Assumes five satellite (minimum) tracked continuously with the recommended antenna using the recommended static surveying procedures utilizing L1 and L2 signals at all sites; precise ephemerides and meteorological data may be required. Performance specifications are RMS and ppm values are times baseline length.

Start-up:	< 30 seconds from power-on to start survey with recent ephemeris
Tracking:	L1 C/A code, L1/L2 full-cycle carrier. Fully operational during P-code encryption.
Number of channels:	Total station: 18 CORS: 24
Data-logging:	In internal memory; in optional TSC1 data collector; or on TSC1 optional removable PC Card
Receiver Data storage:	65 hours internal memory of L1/L2 data, 5 satellites, 15 second interval (typical), Internal memory expandable in steps to over 1,300 hours continuous L1/L2 with average 5 satellites and 15 second interval. 4.5 hours internal memory of L1/L2 data, 5 satellites, 1.0 seconds (minimum)

Table 5.8: General Performance

5.4.2.2. Casing, Connections and Power Supply

Figure 5.9: Trimble 4000 SSe Receiver Front and Rear View (Ruler Scale is 30cm)

Figure 5.10: Trimble Power Unit (220 V AC to 12 V AC) and Battery Charger / Data Link (Ruler Scale is 30 cm)

Power and Power Connection

The Trimble receiver will use 220 V from the power distribution rack panel. The 220 V power cable runs from the power distribution rack panel to the AC/DC converter (220 VAC to 12 VDC) and battery charger. A 12 V power line connects the converter and the receiver. Alternatively, the receiver can be used directly on 28 VDC aircraft power if it is filtered for large spikes and DC-shifts.

5.4.2.3. Trimble 4000 SSi Antennas

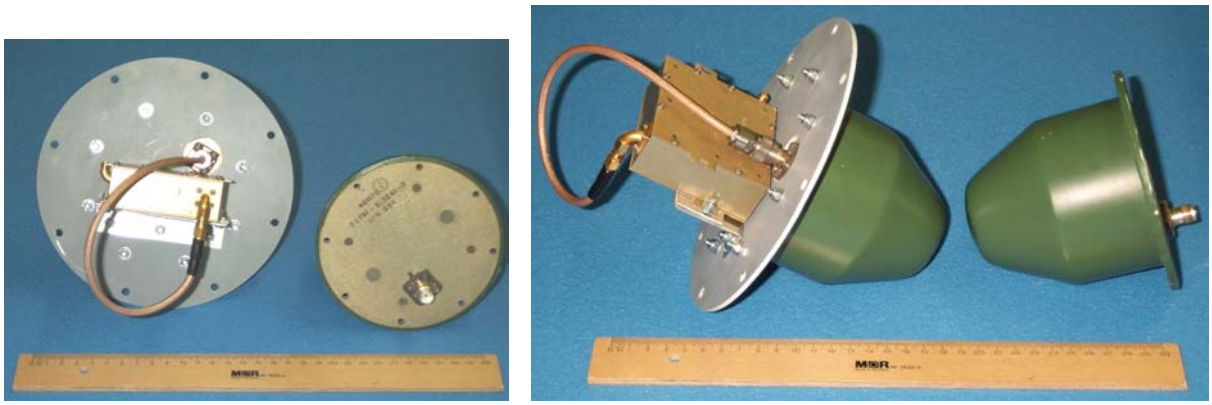

Figure 5.12 : Trimble Aircraft Antenna with and without Adaption Plate and Pre-Amplifier (Ruler Scale is 30cm)

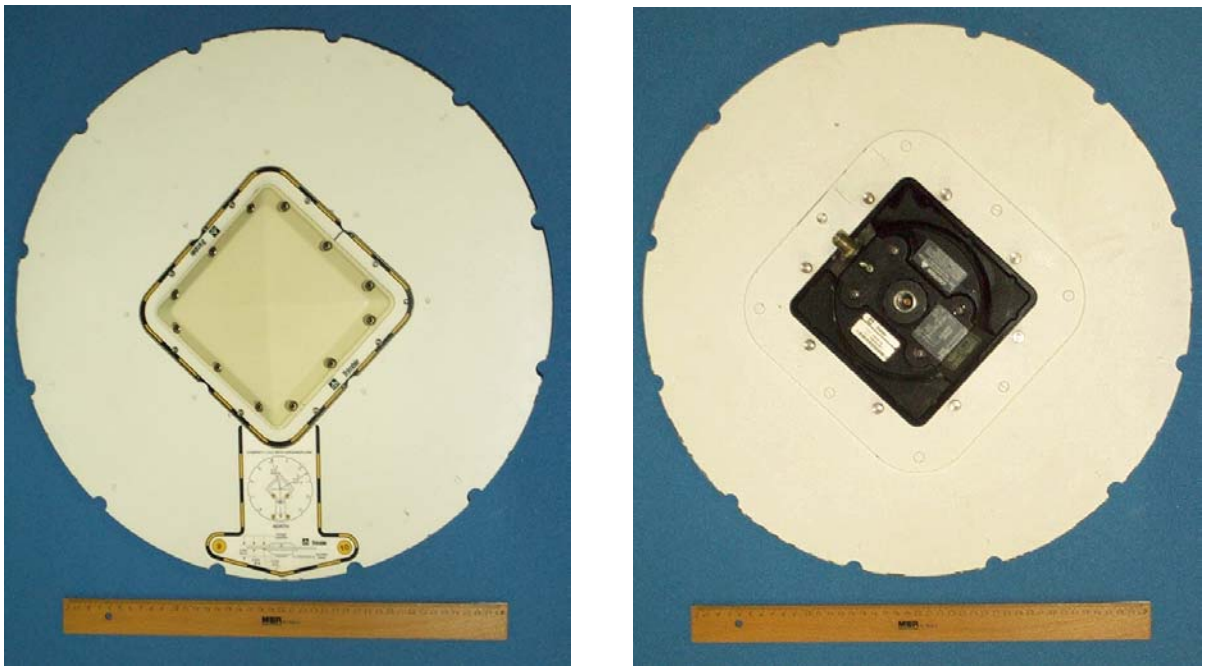

Figure 5.13 : Trimble Static Geodetic Antenna form Top and Bottom (Ruler Scale is 50 cm)

Antenna and Antenna Connection

The Trimble 4000 SSi is connected to a flat-line antenna with an integral LNA via a standard TNC-type female receptible wired for connection via 50-ohm coaxial cabling. The connector shell is connected to the Trimble receiver ground. The TNC-type connector center pin provides +12 VDC (to power the LNA) and accepts 1227 and 1575.42 MHz RF input from the antenna. The RF and DC signals share the same path. The current for the GPS antenna connector is limited to 150 mA out of the center conductor. It is short circuit protected. If using a splitter or other RF network, use an inner DC block suitable for 1 – 2 GHz , 50-ohm. Maximum voltage back to the Trimble receiver cannot exceed 15V.

5.5 Riegl laser altimeter

The Riegl distance meter (Figure 5.10) enables laser range measurements even under conditions of bad visibility. Generally spoken, the distance meter provides the range of the last target, even if the measuring beam partially hits or penetrates other targets before (Figure 5.11). Thus, the technique is addressed as last pulse detection.

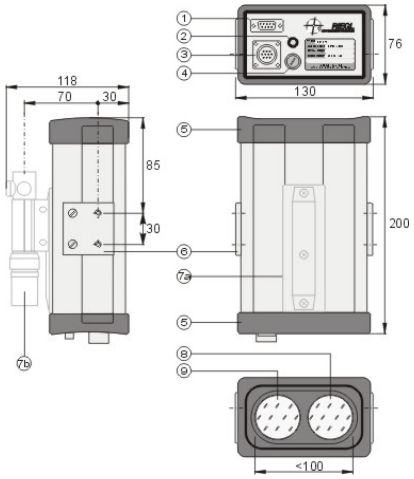

Figure 5.14: Riegl laser altimeter (physical units are mm).

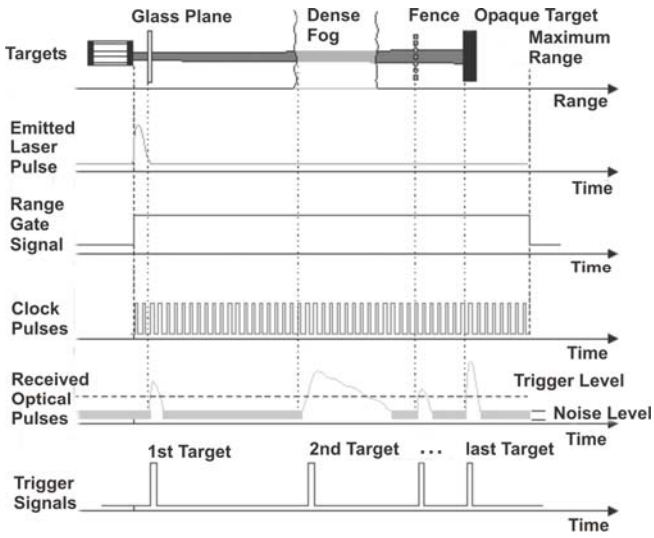

Figure 5.15: Last Pulse Detection

The main features of the laser distance meter are: light weight and stable metal housing, short high-energy infrared light pulses provide excellent interference immunity, measurements are fast offering update rates as high as 200 Hz / 2 kHz / 12 kHz, measurements can be taken through glass windows, narrow measurement beam with very low divergence providing good spatial resolution, measurements can be taken to almost any surface regardless of the incident beam angle or surface characteristics and measurements are unaffected by the temperature of the material surface and of temperature gradients in the medium between the sensor and the target surface. For technical details see Tables 5.7 and 5.8.

Physical size:	13 cm (5”) W x 20 cm (8”) D x 7.6 cm (3”) H
Weight:	approx. 1.5 kg (3.3 lbs)
Power requirement:	approx. 10 Watt @ 11-18 Volts DC protecting circuitry for over-voltage and reverse polarity
Option 20-28 VDC:	external pre-stabilization and protecting module STAB95 (used on aircraft installation)
Option 220 VAC	external power supply module VNG95 (not yet available at GFZ)
Temperature range:	Operation -10° C to +50° C Storage -20° C to +60° C
Protection class:	IP64
Data interfaces:	RS232 & RS422 (selectable, standard for all types) Baud rate selectable between 150 Baud and 19200 Baud, further 38.4 kBaud and 115.2 kBaud RS422 high speed (available for VHS types only) 115.2 kBaud in "high speed" mode, 19.2 kBaud in "adjust" mode, asynchronous Parallel interface (extended capabilities port)
Available data output: (options not for all types) Switching output	Analogue current, 4-20 mA [1], not galvanically isolated, resolution 16 Bit, linearity 0.05 ‰ of full scale 2 x PNP transistor driver [2] built-in thermal and short-circuit protection switching current 250 mA maximum switching voltage = supply voltage

[1] operating range selectable via serial interface
[2] switching points adjustable via serial interface

Table 5.9: Physical properties of the Riegl laser altimeter

Measuring range (depending on the reflection coefficient of the target):	
good, diffusely reflecting targets, reflectivity ³:	80 up to 500 m [1]
bad, diffusely reflecting targets, reflectivity ³ 10%:	up to 150 m [1)]
reflecting foil [2] or plastic cat's-eye reflectors:	> 1000 m
Minimum distance:	typically 5 - 10 m
Distance measurement accuracy [3]:	typically ±5 cm Worst-case ±10 cm
Measuring time (ms or s) [4]:	10ms / 20ms / 50ms / 0.1 / 0.2 / 0.5 / 1 / 2
Statistical deviation (cm) [5]:	±10 / ±7 / ±5 / ±3 / ±2 / ±1.5 / ±1 / ±0.7
Resolution [5, 6]:	10 / 10 / 5 / 5 / 2 / 2 / 1 / 1
Measuring time, typically [4]:	0.5 s
Divergence of the infrared measuring beam [7]:	1.8 mrad
Eye safety class:	according to CENELEC EN 60825-1 (1997)

[1] Typical values for average conditions. In bright sunlight, the operational range is considerably shorter than under an overcast sky. At dawn or at night the range is even higher.
[2] Reflecting foil 3M 2000X or equivalent, minimum dimensions 0.45 x 0.45 m2.
[3] Standard deviation, plus distance depending error < 20 ppm.
[4] Adjustable via RS232.
[5] Depending on measuring time.
[6] Chosen automatically by the internal microprocessor.
[7] 1 mrad corresponds to 10 cm beam width per 100 m of distance.

Table 5.10: Performance parameters of the Riegl laser altimeter

Power distribution and control

The main power sources are the power generators connected to the aircraft engines. The generators supply a noisy, slightly fluctuating 28 VDC. A voltage inverter is used to transform the primary 28 VDC into 230 VAC. This secondary power source provides the PC104 systems and the strap-down gravity meter. The LaCoste & Romberg meter has its own unbreakable power supply unit that is fed with 230 VAC and distributes 115 VAC to the sensor and PC system. The laser altimeter and the central time trigger unit have their own DC/DC converters; both systems can be directly supplied by the primary 28 VDC.

6 Ground equipment

6.1 LaCoste & Romberg G-meter

In order to link the relative airborne gravity measurements to a regional gravity reference system, a LaCoste & Romberg G-meter (Figure 6.1) was used. The instrument is owned by the UNAM and was operated by Mario Rebolledo.

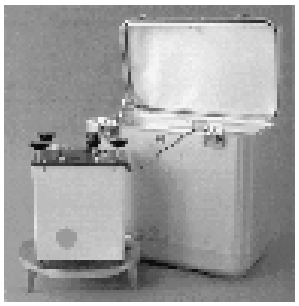

Figure 6.1: LaCoste & Romberg G-meter

6.2 Trimble / Ashtech GPS receivers

See previous chapter.

6.3 Computer systems

Several more computers are needed in a temporal office in order to ensure data storage, quality control etc. One laptop is reserved for data copying, temporal storage and CD-burning. In this case, data copying includes the conversion of binary data of individual sensors into ASCII formats (as the transformation of binary GPS observation data to RINEX files). This computer needs flash-card readers, CD-burner connection and extended memory. A second laptop is in use for data evaluation as the testing of the quality of GPS data and the computation of first gravity profiles. A third laptop is linked to the Internet in order to download GPS ephemeredes and to function as small mail-server. Another laptop is reserved for the pilots for flight planning and download of meteorological data. For flight planning the internationally used program FliteStar is used. At last, one laptop is necessary to control and maintain the stations in the field and to download long term GPS data at remote stations.

7 Aeromagnetometry data

7.1 Data acquisition

The CRM aeromagnetometry system was permanently installed in the aircraft. CRM scientists took the responsibility to conduct the measurements in the air and on ground. The system consists of a Scintrex cesium vapor magnetometer system for total field ground measurements and a GEM cesium system for the airborne use. The airborne sensor was installed in the rear part of the tail stinger mounted to the aircraft.

7.2 Data processing

The aeromagnetometry data has been pre-processed at GFZ using the program package GeoSoft™. IGRF2000 reduction and an upward continuation to a common flight level based on Hansen und Miyasaki (1984) to a common height level was applied using self-written software.

7.3 Data imaging

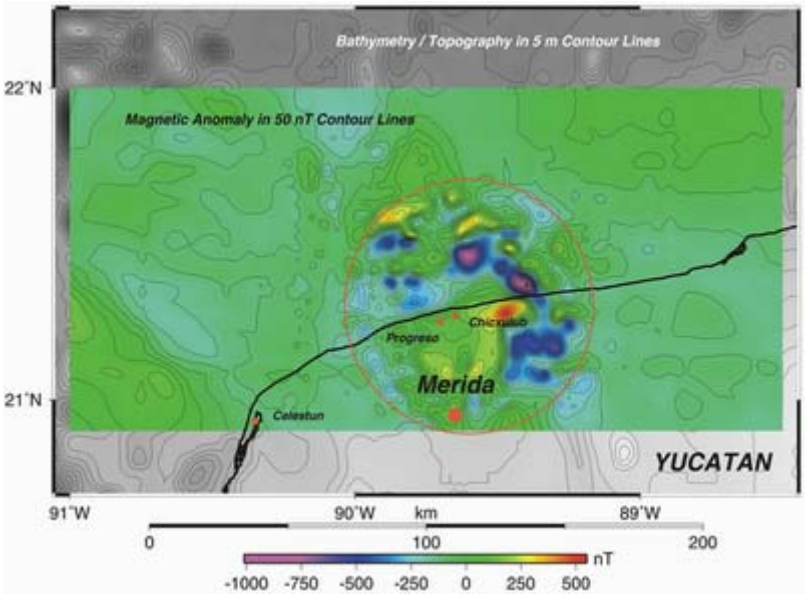

Figure 7.1: Map of the total field magnetic anomaly of the Chicxulub impact structure (in color), overlain on the topographic / bathymetric structures (gray shaded).

Figure 7.2 : (next page) 3D-views on the total field magnetic anomaly. From top to bottom: 45° view angle, 135° view angle, 225° view angle and 315° view angle.

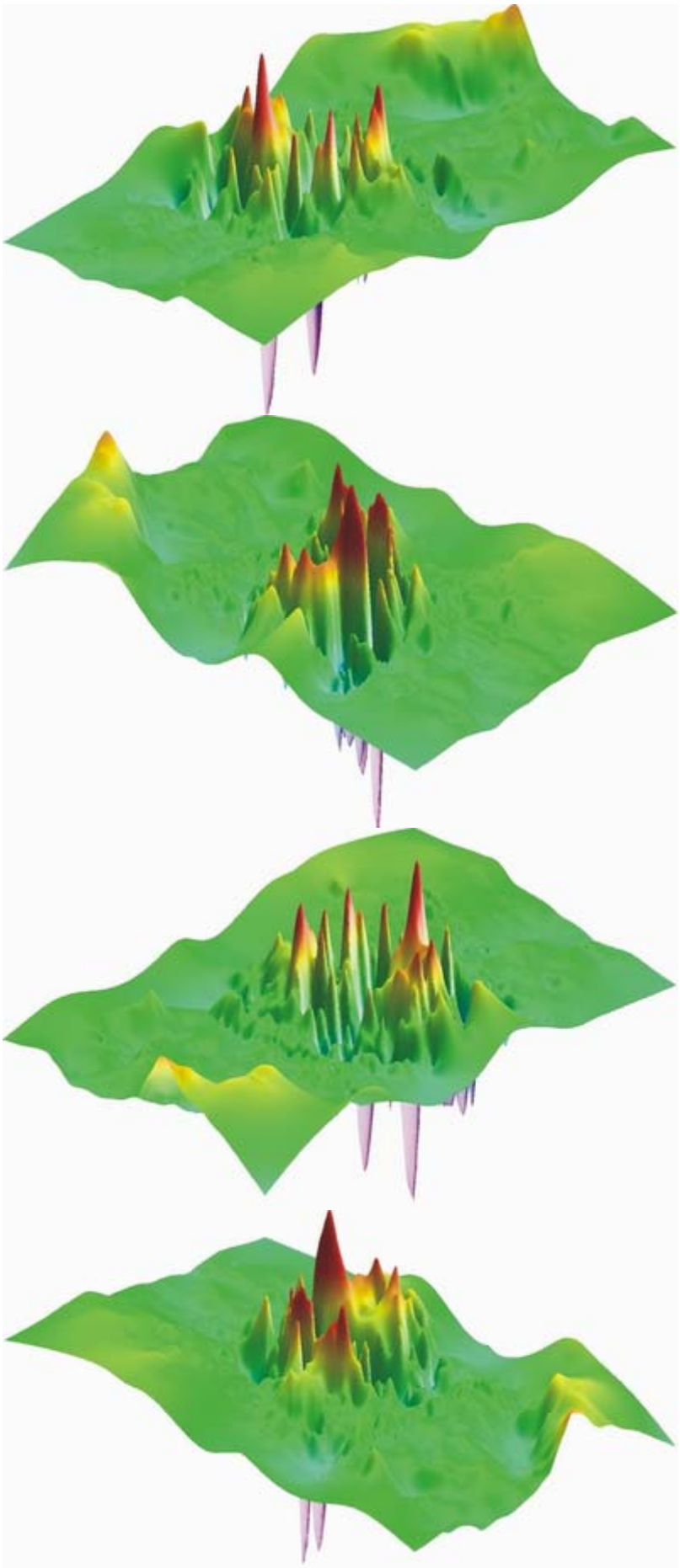

8 Gravity processing

A schematic image about the concept of airborne gravimetry is given in Figure 7.1. An overview about the aerogravimetry data processing is given in Figure 7.2. In the initial phase of the data processing, the kinematic differential GPS data is computed. In our case we used the GeoGenius software for this purpose. Only in cases where GeoGenius gave no results due to internal errors, the KSG-Soft program [Xu et al, 1998] was used. Comparisons between both software solutions on profiles without errors or data uncertainties showed good agreement. The second primary data input is the raw gravity measurement from the LaCoste & Romberg gravity meter. One of the first crucial steps in GPS data processing is the determination of time offsets between GPS and other input data. In order to accurately estimate the time offset the GPS time is defined as correct and fixed. From the GPS heights the vertical aircraft acceleration are computed. This is the reference for the time correlations to follow. The data stream (for instance of the gravity data) is first shifted within a time window of some minutes and later on in window of some seconds in order to find the best time correlation. Finally, the best time correction over the full profile length is determined, assuming a static shift. If for some reason time fluctuations are suspected in a time series, a dynamic data shift for each epoch based on a 30 seconds window is can be optionally computed. The more and the steeper gradients occur in the data set, the better the time correlation will work. Of course, such strong disturbances are generally not desirable. The software is able to fit the data streams up to a 1/100 second. After the synchronization is ensured, the Eötvös correction, tilt correction and, if required, free-air reduction is computed. All these computations are still based on the unfiltered, common 1 Hz data frame. Only after all corrections and reductions are applied, the data is low-pass filtered using a Butterworth filter with a cut-off wavelength of 240 seconds, translating to a mean spatial resolution of about 6.5 km. Details of the processing are given in Meyer et al. [2003].

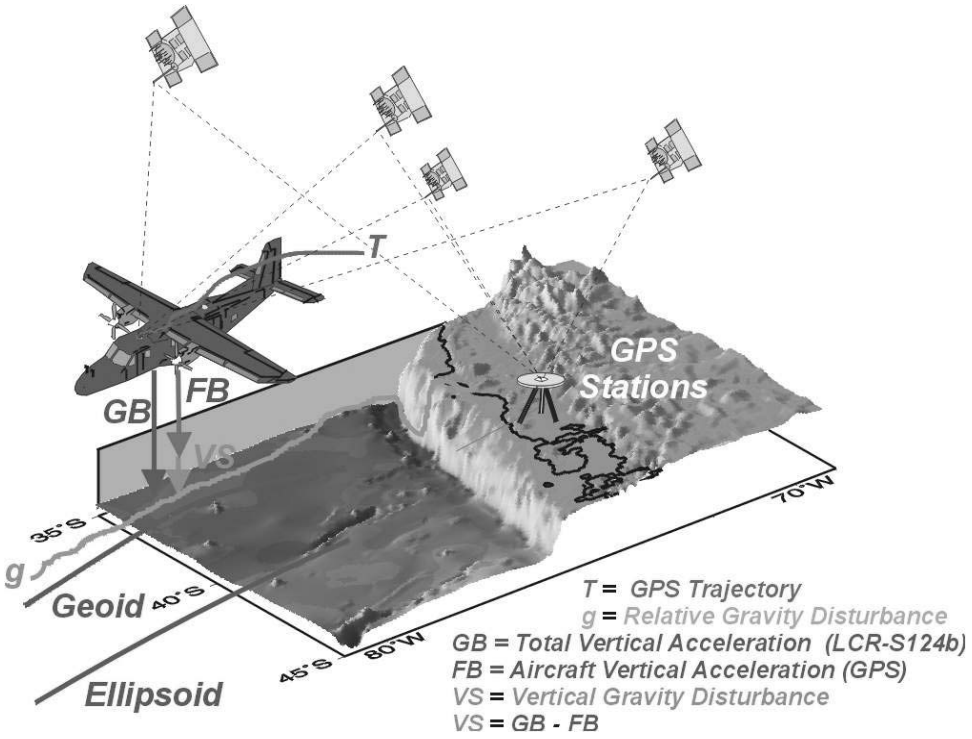

Figure 7.1: Overview about the concept of airborne gravimetry.

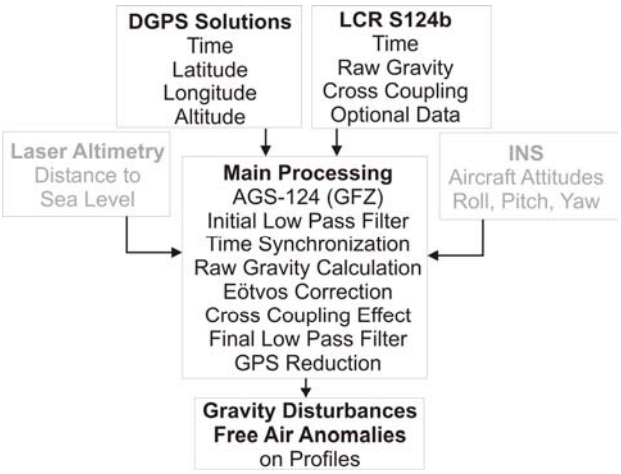

Figure 7.2: Overview about airborne gravimetry processing. Optional data inputs to the processing are given in gray.

For ground truth comparison three data sets the results of the Mexico'97 was used.

In order to keep the resulting data comparable between profiles, a constant k-factor of 38.5 was used to scale the gravity data instead of optimizing the k-factor for each flight. Offshore and onshore free-air correction was computed without including terrain effects.

In conclusion, the effect of some small meter errors multiplied by relatively large aircraft disturbances due to the lack of an auto-pilot (vertical aircraft accelerations were a factor of 5 to 10 higher than with a comparable aircraft using an auto-pilot) resulted in a broadened error margin for the airborne gravity data. The quality of the individual profiles is discussed in the subsequent chapters.

The strap-down gravity meter data will be presented in a future publication and is not discussed here.

9 Aerogravity profiles from Zacatecas

Comments:

First resolvable flight from Zacatecas.
Prior flights were test flights.

As all following flights ex Zacatecas the time on profile was very short (~ 30 minutes), therefore the spatial coverage and resolution is low.

All flights from Zacatecas were requested in this manner by CRM.

The shown profile shows good accordance to ground truth data.

Comments:

Second resolvable flight from Zacatecas.

As all following flights ex Zacatecas the time on profile was very short (~ 30 minutes), therefore the spatial coverage and resolution is low.

All flights from Zacatecas were requested in this manner by CRM.

The shown profile shows good accordance to ground truth data.

Comments:

Second resolvable flight from Zacatecas.

As all following flights ex Zacatecas the time on profile was very short (~ 30 minutes), therefore the spatial coverage and resolution is low.

All flights from Zacatecas were requested in this manner by CRM.

After turbulences, the shown profile shows good accordance to ground truth data.

Comments:

Second resolvable flight from Zacatecas.
Prior flights were test flights.

As all following flights ex Zacatecas the time on profile was very short (~ 30 minutes), therefore the spatial coverage and resolution is low.

All flights from Zacatecas were requested in this manner by CRM.
Extremely short profile.
After turbulences, the shown profile shows good accordance to ground truth data.

Comments:

Third resolvable flight from Zacatecas.

As all following flights ex Zacatecas the time on profile was very short (~ 30 minutes), therefore the spatial coverage and resolution is low.

All flights from Zacatecas were requested in this manner by CRM.
Longest profile from Zacatecas.
The shown profile shows good accordance to ground truth data.

10 Merida aerogravimetry profiles

Comments:

First survey flight from Merida.

Prior flights were test and transfer flights.

The shown profile shows high deviation from ground truth data due to too strongly fixed rubber strings at lower graviymeter frame.

Additional offset problems in GPS and INS data.

Comments:

First survey flight from Merida.

Prior flights were test and transfer flights.

The shown profile shows some deviation from ground truth data due to too strongly fixed rubber strings at lower graviymeter frame.

Comments:

First survey flight from Merida.

Prior flights were test and transfer flights.

The shown profile shows some deviation from ground truth data due to too strongly fixed rubber strings at lower graviymeter frame.

Comments:

First survey flight from Merida.

Prior flights were test and transfer flights.

The shown profile shows high deviation from ground truth data due to too strongly fixed rubber strings at lower graviymeter frame.

Strong turbulences at coast / water transition.

Comments:

Second survey flight from Merida.

The shown profile shows good correlation with ground truth data.

Relatively smooth flight conditions.

Comments:

Second survey flight from Merida.

The shown profile shows good correlation with ground truth data, except one data bump at about 1700 seconds.

Relatively smooth flight conditions.

Comments:

Second survey flight from Merida.

The shown profile shows good correlation with ground truth data.

Relatively smooth flight conditions.

Comments:

Third survey flight from Merida.

The shown profile shows some deviation from the ground truth data.

Relatively rough flight conditions.

Comments:

Third survey flight from Merida.

High disturbance because of flight level change and beam clamping at about 1500 seconds.

Relatively rough flight conditions.

Comments:

Third survey flight from Merida.

The shown profile shows significant deviation from the ground truth data.

Rough flight conditions.

Comments:

Fourth survey flight from Merida.

The shown profile shows significant deviation from the ground truth data.

Rough flight conditions.

Comments:

Fourth survey flight from Merida.

The shown profile shows some deviation from the ground truth data.

Very rough flight conditions.

Comments:

Fifth survey flight from Merida.

The shown profile shows significant deviation from the ground truth data.

Short profile, rough flight conditions.

Comments:

Fifth survey flight from Merida.

The shown profile shows good correlation with the ground truth data.

Rough flight conditions.

Comments:

Fifth survey flight from Merida.

The shown profile shows good correlation with the ground truth data.

Relatively good flight conditions.

Comments:

Sixth survey flight from Merida.

The shown profile shows good correlation with the ground truth data.

Relatively smooth flight conditions.

Comments:

Sixth survey flight from Merida.

The shown profile shows hiogh deviations from the ground truth data.

Short profile, flight level change, very rough flight conditions.

Comments:

Sixth survey flight from Merida.

The shown profile shows good correlation with the ground truth data.

Relatively smooth flight conditions away from the coastline.

Comments:

Seventh survey flight from Merida.

The shown profile shows good correlation with the ground truth data.

Relatively smooth flight conditions.

Comments:

Seventh survey flight from Merida.

The shown profile shows some deviation from the ground truth data.

Relatively rough flight conditions.

Comments:

Eigth survey flight from Merida.

The shown profile some deviations from the ground truth data.

Rough flight conditions.

Comments:

Seventh survey flight from Merida.

The shown profile shows good correlation with the ground truth data.

Relatively rough flight conditions.

Comments:

Eigth survey flight from Merida.

The shown profile shows good correlation with the ground truth data except for high frequency noise.

Partly rough flight conditions.

Comments:

Eigth survey flight from Merida.

The shown profile high diturbance in comparison to the ground truth data except for high frequency noise.

Very rough flight conditions.

Comments:

Nineth survey flight from Merida.

The shown profile shows good correlation with the ground truth data except for high frequency noise.

Partly rough flight conditions.

Comments:

Nineth survey flight from Merida.

The shown profile shows good correlation with the ground truth data except for high frequency noise.

Partly rough flight conditions.

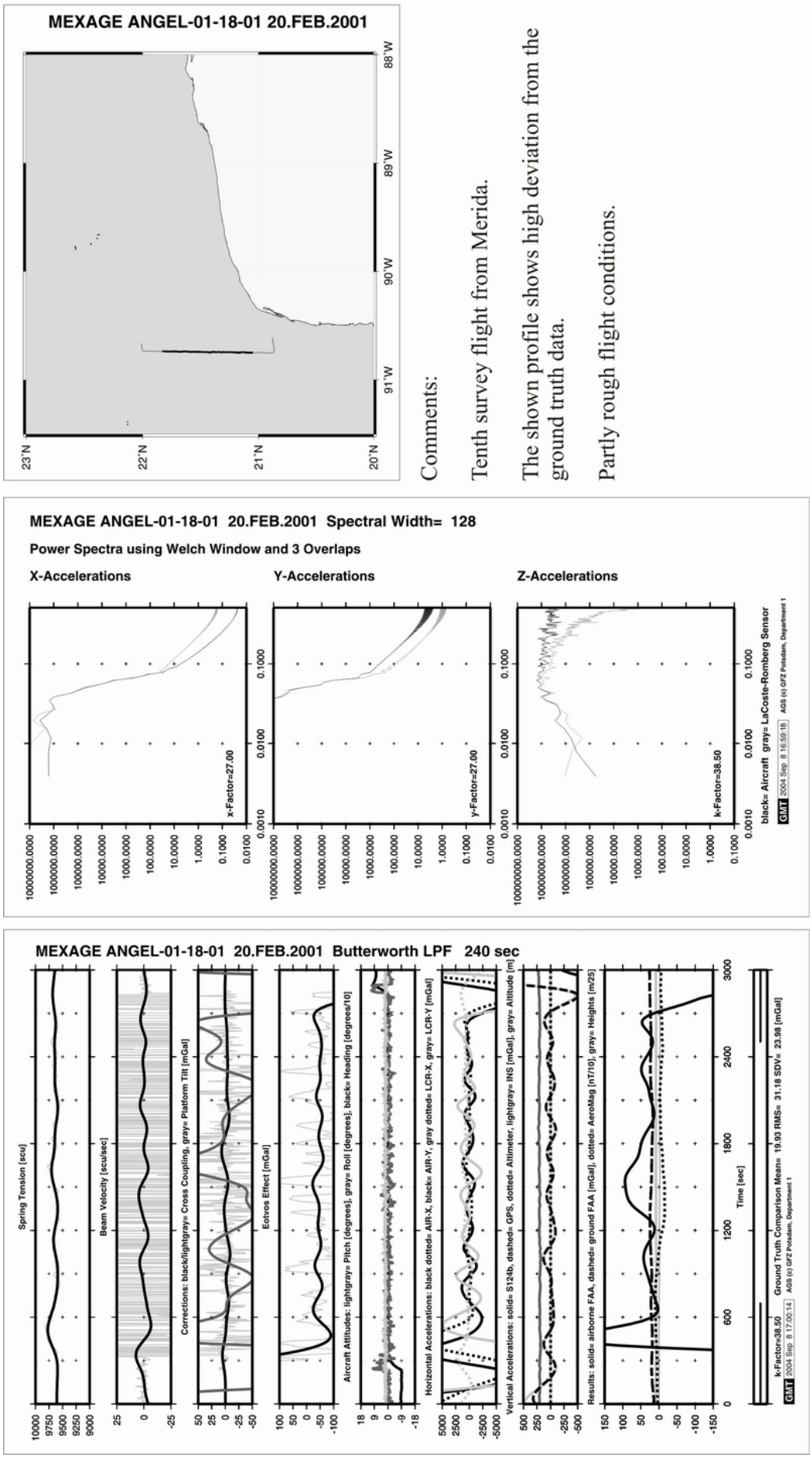
MEXAGE ANGEL-01-18-01 20.FEB.2001
23°N
22°N
21°N
20°N
91°W
90°W
89°W
88°W
Comments:
Tenth survey flight from Merida.
The shown profile shows high deviation from the ground truth data.
Partly rough flight conditions.
MEXAGE ANGEL-01-18-01 20.FEB.2001 Spectral Width= 128
Power Spectra using Welch Window and 3 Overlaps
X-Accelerations
Y-Accelerations
Z-Accelerations
x-Factor=27.00
y-Factor=27.00
k-Factor=38.50
black= Aircraft gray= LaCoste-Romberg Sensor
GMT 2004 Sep 8 16:59:18 AGS (e) GFZ Potsdam, Department 1
MEXAGE ANGEL-01-18-01 20.FEB.2001 Butterworth LPF 240 sec
Spring Tension [scu]
Beam Velocity [scu/sec]
Corrections: black/lightgray= Cross Coupling, gray= Platform Tilt [mGal]
Eotvos Effect [mGal]
Aircraft Attitudes: lightgray= Pitch [degrees], gray= Roll [degrees], black= Heading [degrees/10]
Horizontal Accelerations: black dotted= AIR-X, black= AIR-Y, gray dotted= LCR-X, gray= LCR-Y [mGal]
Vertical Accelerations: solid= S124b, dashed= GPS, dotted= Altimeter, lightgray= INS [mGal], gray= Altitude [m]
Results: solid= airborne FAA, dashed= ground FAA [mGal], dotted= AeroMag [nT/10], gray= Heights [m/25]
Time [sec]
k-Factor=38.50 Ground Truth Comparison Mean= 19.93 RMS= 31.18 SDV= 23.98 [mGal]
GMT 2004 Sep 8 17:00:14 AGS (e) GFZ Potsdam, Department 1

Comments:

Tenth survey flight from Merida.

The shown profile shows high deviation from the ground truth data.

Partly rough flight conditions.

Comments:

Eleventh survey flight from Merida.

The shown profile shows good correlation with the ground truth data.

Smooth flight conditions.

Comments:

Eleventh survey flight from Merida.

The shown profile shows good correlation with the ground truth data.

Smooth flight conditions.

Comments:

Eleventh survey flight from Merida.

The shown profile shows some deviation from the ground truth data.

Smooth flight conditions.

Comments:

Twelveth survey flight from Merida.

The shown profile shows good correlation with the ground truth data except for some data bumps.

Mostly smooth flight conditions.

Comments:

Twelveth survey flight from Merida.

The shown profile shows good correlation with the ground truth data except for high frequency noise.

Rough flight conditions.

Comments:

Fourteenth survey flight from Merida.
Thirteenth flight could not be resolved due to permanently clamped beam during flight.

The shown profile shows good correlation with the ground truth data except for some data bumps.

Mostly rough flight conditions.

Comments:

Fourteenth survey flight from Merida.
Thirteenth flight could not be resolved due to permanently clamped beam during flight.

The shown profile high deviations from the ground truth data.

Veryy rough flight conditions.

Comments:

Fourteenth survey flight from Merida.
Thirteenth flight could not be resolved due to permanently clamped beam during flight.

The shown profile shows good correlation with the ground truth data except for some data bumps.

Mostly rough flight conditions.

Comments:

Fifteenth survey flight from Merida.

The shown profile shows partly good correlation with the ground truth data except for some data bumps.

Mostly rough flight conditions.

Comments:

Fifteenth survey flight from Merida.

The shown profile shows high deviations from the ground truth data

Very rough flight conditions.

11 Acknowledgements

The MEXAGE survey would not have been possible without the work of the ICDP working group on the Chicxulub crater. This team laid the grounds for the survey.

Prof. Urrutia-Fucugauchi of the UNAM was our most important partner in Mexico. He cared about the financial investments and made contact with CRM to use their aircraft. He also made available some students to set up GPS base station at the early part of the survey.

Most essential for the practical field work and all logistic set-ups was Mario Rebolledo. Mario kept his friendly and helpful attitude throughout the entire survey.

We are obliged the thank the team of the CRM that helped to install our instruments on their aircraft and cared for pilots, scientists, technicians and everyday help. Especially the science team was joyful to work with. The pilots had to endure long and boring flights without loosing their grip and concentration. They managed to do a good job. The technicians kept the aircraft running at all times, even in the hottest days.

We thank Dr. Gerd Boedecker for making available the SAGS instrumentation and the extra written program code to run it easily on laptops.

Last not least we thank the executive board of the GFZ, Prof. Emmermann and Dr. Raiser, the head of Department 1, Prof. Reigber and the head of Section 1.3, Dr. Schwintzer for their support of the survey.

12 Annex 1

Agreement on Geoscience Cooperation
between the
Universidad Nacional Autonoma de Mexico
and the
GeoForschungsZentrum Potsdam of the Federal Republic of Germany

November 1999

The National University of Mexico City (hereinafter referred to as UNAM), as represented by Prof. Dr. Francisco Barnés de Castro, Rector de la UNAM and Dr. Francisco Bolívar Zapata, Dean of Research of UNAM, and the GeoForschungsZentrum Potsdam, Germany (hereinafter referred to as GFZ), as represented by Prof. Dr. Rolf Emmermann, Scientific Executive Director of GFZ and Dr. Bernd Raiser, Administrative Executive Director of GFZ,(hereinafter referred to as "The Parties") have reached a bilateral cooperation agreement as follows:

Fields of Scientific Cooperation

1. The parties agree that the cooperation as referred to in this agreement may include, but is not limited to, the following activities:

- Cooperation on the Chicxulub Scientific Drilling Program within the framework of the International Continental Scientific Drilling Program.
- Cooperative research on geosciences, including environmental studies, especially on the application of satellite remote survey and management, the application of Global Positioning System (GPS) in the crustal and lithospheric deformation monitoring, the recovery of palaeo-climate and palaeo-environmental records from continental sediments, the review and mitigation of geological hazards**,** *lithosphere study and the management of geoscientific data.*
- Cooperation in seismological survey by broad band volcanic seismology, high resolution deformation survey by GPS and installation of gas monitoring systems on the volcanoes Popocatepetl and Colima.
- Academic exchange between scientists and joint training programs for scientists and technicians.

2. If necessary, the parties will hold annual discussion meetings on detailed issues and workplans.

Implementation of Cooperation

1. The cooperation carried out under the agreement will be subject to the funds and staff available to the parties.
2. GFZ's activities under the agreement will be subject to the management and supervision of the Executive Board of the GFZ.
3. The scientific cooperation of UNAM under the agreement will be subject to the management of the Office of the Dean of Research.
4. The scientific activities of UNAM under the agreement will be carried out and are the responsibility of the Institute of Geophysics.

Right to Use the Cooperative Research Results

1. The parties will share the use of the non-exclusive and non-monopolized copyrights and patents achieved through the cooperative research at no additional cost.
2. In case of the transmitting of the right to use the cooperative results to a third party by one party, the other party's approval must be obtained.

Supervision of Cooperative Research Activities

The parties shall each designate a representative to amend the cooperative research objectives and activities on mutual consent. The representatives shall meet according to need. The activity report for the previous year and workplan for the second year will be exchanged annually. Except for the particular projects that shall be agreed upon through writing, the parties shall amend annually plans independently. The party that makes amendment to the plan shall notify the other party on decisions and on objectives concerning continuing cooperation.

Publications

The parties agree that the publications of cooperative results by one party must proceed with the approval of the other party.

Dispute Resolution

All disputes that arise as a result of the International Scientific Cooperation Agreement, related to the agreement, or the breach of the agreement shall be resolved through consultation. In case when the parties cannot agree six months after the dispute arises, the agreement shall be terminated.

Obligations

The agreement shall not conflict with international laws and domestic laws of the parties.

Implementation and Termination

The agreement will enter effect upon signature and shall remain in force for a period of 5 years. It may be extended by mutual agreement for another 5 years.
The agreement may be amended or expanded by mutual agreement in writing. It may be terminated upon 90 days notice to the other party by the party proposing the termination. The termination of the agreement shall not affect the effectiveness and duration of projects agreed upon the parties and already in operation before termination.

This agreement is signed in English in Mexico City on November 5, 1999.

Signed,

on behalf of UNAM:	Dr. Francesco Bolívar Zapata, Dean of Research
	Dr. Jaime Urrutia Fucugauchi, Institute of Geophysics
on behalf of GFZ:	Prof. R. Emmermann, Scientific Executive Director

13 Annex 2

Agreement on Geoscience Cooperation I
between Universidad Autónoma de México
and the GeoForschungsZentrum Potsdam of the Federal Republic of Germany

November 17, 1999

Technical Appendix

The use of space-borne geodetic techniques, telecommunication and data networks has recently made possible the development of real-time or nearly real-time monitoring of geological and geophysical processes. On the other hand, advances on GPS-based geodetic techniques provide the potential for making fundamental advances in volcanology because ground deformation occurs almost inevitably before volcanic eruptions.

Evidence from many volcanoes shows that the ground motion reflecting changes on magma chamber physical and chemical conditions can be detected months or weeks in advance and precede even seismic activity or other eruption precursors.

Given the high risk situation and potentially catastrophic situations derived from the activity of volcanoes, GFZ and UNAM have jointed efforts in order to develop PUMAS (Permanent Universal Monitoring GPS Array System) that may be used both as an early warning system and as a tool for a better understanding on active volcanoes.

The activities planned within this agreement are summarized as follows:

a) Development, installation, operation and maintenance of PUMAS, a GPS-based system that will be used to record surface deformation and as a precursor for volcanic activity.
b) PUMAS will be set-up on Popocatepetl and Colima volcanoes, where it will undergo initial test.
c) PUMAS will be susceptible to be complemented with other geophysical monitoring instruments. It is intended to be a backbone upon which multiple geophysical instruments can be remotely located and provide real-time information that may be of importance for geological hazard evaluation.
d) Popocatepetl and Colima are targeted as initial feasibility targets but given a successful operation, expansion of the network may be considered, given volcanic activity in other areas and available funds from GFZ AND / or UNAM.

1. Responsibilities of GFZ

1.1 The GFZ will provide a complete monitoring system (hardware and software), ready for installation and automatic continuous operation.
1.2 GFZ is responsible to achieve the necessary licenses for temporary export of the equipment from Germany.
1.3 GFZ will deliver spare parts.
1.4 Shipping expenses to Mexico and back to Germany will be covered by GFZ.
1.5 Installation costs, construction and travel expenses of German partners will also be covered by GFZ.

2. Responsibilities of UNAM

2.1 UNAM will serve as a liaison with Mexican civil protection agencies.
2.2 UNAM will cover custom expenses.
2.3 UNAM will ensure that the equipment is in a secure location where it cannot be damaged or stolen.
2.4 UNAM is responsible for obtaining a permission for tax free temporary importation (or will cover customs expenses) of the equipment into Mexico and its subsequent re-exportation.
2.5 UNAM will support the installation and continuous reliable day-by-day operation of the GPS-array.
2.6 UNAM carries responsibility for making available a permanent link to the array's computer via University Campus Local Area Network, using FTP- and Telnet-services.

3. Mutual Responsibilities

Data Processing and interpretation of data generated by PUMAS network will be jointly carried out by GFZ and UNAM. Both parties will freely exchange data and information derived from its operation.
Data distribution to other parties needs written mutual agreement of both GFZ and UNAM.

Potsdam, January 21, 2000
Prof. Dr. R. Emmermann
Dr. B. Raiser

14 Annex 3

Agreement on Geoscience Cooperation II
between Universidad Autónoma de México
and the GeoForschungsZentrum Potsdam of the Federal Republic of Germany

November 5, 1999

Technical Appendix:
Aerogeophysical Survey over the Chicxulub Impact Structure

General Description of Work

A joint airborne survey, covering aeromagnetics and aerogravity over the marine coastal area of the Chicxulub impact structure and the northern part of the Yucatan peninsula shall be carried out by UNAM / Bureau of Mines and GFZ.

Additionally, a mountainous test area defined by the Bureau of Mines shall be surveyed using the GFZ aerogravity equipment.

Chicxulub Impact Structure
The circle-like Chicxulub impact structure on the northern coast of the Yucatan peninsula is most probably caused by a meteorite crash just close to the begin of the Tertiary. The aerogeophysical survey proposed in this area should have flight altitudes of about 50 m above sea level offshore and about 150 m onshore. The main target is to close the data gap of about 30 km from the shoreline towards the north plus a considerable overlap with existing marine profiles and land surveys. The profiles should be flown in E-W direction with perpendicular tielines for survey control. Furthermore, a couple of flight profiles should tie the target area with other existing data as seismic lines and drill sites. For aerogravity, a line spacing of 3 NM is proposed. Tielines should be flown with a spacing of 30 NM for aerogravity. This grid can be easily filled in with more aeromagnetics flights if desired. At least 3 GPS-ground reference stations will be set-up for the survey.

Mountainous Test Area
A mountainous test area defined by the Bureau of Mines will be surveyed using the GFZ aerogravity equipment. The area selected corresponds to Aguascalientes-Zacatecas

Description of Activities

An aircraft of the Bureau of Mines equipped with an aeromagnetics sensing system shall be additionally equipped with an aerogravity system owned by GFZ.
Thus equipped, an aerogeophysical survey over the Chicxulub impact structure shall be carried out. Ground reference stations for GPS and geomagnetics will be distributed and operated in the survey area.
Base of operation will be Merida Airport.
Besides the airborne survey of the southern Gulf of Mexico and the northern Yucatan peninsula, a test survey over the Mexican Highlands shall be carried out.
Base of operation will be the Aguascalientes Airport.

4. Responsibilities of GFZ

4.1 The GFZ will provide an airborne gravity system (hardware and software), ready for installation and operation.
4.2 The GFZ will provide GPS-ground-reference stations for the Chicxulub impact structure survey.
4.3 GFZ is responsible to achieve the necessary licenses for temporary export of the aerogravity equipment from Germany.
4.4 GFZ will bring sufficient spare parts to secure the survey.
4.5 Shipping expenses to Mexico and back to Germany will be covered by GFZ.
4.6 Aircraft installation costs, necessary construction or modification work on the aerogravity system and travel expenses of German partners will also be covered by GFZ.
4.7 GFZ is responsible for GPS and aerogravity data evaluation during the survey.
4.8 GFZ is responsible for all data storage related to the aerogravity system.

5. Responsibilities of UNAM / Bureau of Mines

5.1 UNAM will serve as a liaison with customs.
5.2 UNAM will serve as a liaison with the Bureau of Mines.
5.3 UNAM / Bureau of Mines will serve as liaison with the Mexican Airport and Aviation Authorities.
5.4 UNAM / Bureau of Mines is responsible for obtaining a permission for tax free temporary importation (or will cover customs expenses) of the equipment into Mexico and its subsequent re-exportation.
5.5 UNAM / Bureau of Mines will ensure that the equipment will be stored in a secure location where it cannot be damaged or stolen.
5.6 UNAM / Bureau of Mines will assist on installation of the aerogravity system on an aircraft of the Bureau of Mines and on getting all necessary permits to operate it. The costs of the aircraft operation are paid by UNAM.
5.7 UNAM / Bureau of Mines will ensure flight permits over the survey area.
5.8 UNAM / Bureau of Mines will assist in setting up ground based GPS-reference stations.
5.9 Bureau of Mines is responsible for aeromagnetics instrumentation and measurements as well as for data storage related to aeromagnetics.
5.10 Bureau of Mines is responsible for the set-up of GPS-ground-reference stations for the test survey over a mountainous area.

6. Mutual Responsibilities

6.1 Data Processing and interpretation of data generated by the airborne survey will be jointly carried out by GFZ and UNAM / Bureau of Mines.
3.2 Both parties will freely exchange data and information derived from its operation.
3.3 Data distribution to other parties needs written mutual agreement of both GFZ and UNAM / Bureau of Mines.
3.4 The layout of the flight profiles will be jointly discussed and agreed upon.
3.5 All survey flights will be conducted according to the rules of the Mexican Aviation Authorities.
3.6 UNAM / Bureau of Mines and GFZ will name scientists and engineers responsible for the sub-tasks of the airborne survey.

15 References

Andersen, O. B. , Knudsen, P., 1998: Global marine gravity field from the ERS-1 and Geosat geodetic mission altimetry, J. Geophys. Res. Vol. 103 , No. C4 , p. 8129 (97JC02198)

Campos-Enriquez, J. O., Morales-Rodriguez, H.-F., Domíngez-Mendez, F., Birch, F. S., 1998: Gauss' theorem, mass deficiency at the Chicxulub crater (Yucatan, Mexico) and the extinction of the dinosaurs, Geophysics, Vol. 63, No. 5, 1585-1594

Espindola, J. M., Mena, M., de la Fuente, M., Campos-Enriquez, J. O., 1995: A model of the Chicxulub impact structure (Yucatan, mexico) based on its gravity and magnetic signatures, Physics of the Earth and Planetary Interiors, 92, 271-278

ETOPO'2 Global Relief Data CD-Rom, NOAA'S National Geophysical Data Center, 325 Broadway , E/GC4, Boulder, Colorado 80303-3328 U.S.A.

GLOBE 1 km global terrain model CD, World Data Center-A, National Geophysical Data Center, 325 Broadway , E/GC4, Boulder, Colorado 80303-3328 U.S.A.

GTOPO'30 CD, EDC DAAC User Services, EROS Data Center, Sioux Falls, SD 57198 USA

Hildebrand, A. R., Pilkington, M., Ortiz-Aleman, C., Chavez, R. E., Urrutia-Fucugauchi, J., Connors, M., Graniel-Castro, E., Camara-Zi, A., Halpenny, J. F., Niehaus, D., 1998: Mapping Chicxulub crature structure with gravity and seismic reflection data, in: Graday, M. M., Hutchinson, R., McCall, G. J. H., Rothery, D. A. (eds): Meteorites: Flux with Time and Impact Effects, Geological Society, London, Special Publications, 140, 155-176

LaCoste, L. J. B., Clarkson, N. and Hamilton, G., 1967: LaCoste & Romberg stabilized platform shipboard gravity meter, Geophysics, 32, 99–109

LaCoste, L. J. B., 1988: The zero-length spring gravity meter, Geophysics, 7, 20–21

Marchenko, A. N., Barthelmes, F., Meyer, U., Schwintzer, P., 2001: Regional Geoid Determination: An Application to Airborne Gravity Data in the Skagerrak, Scientific Technical Report STR01/07, GeoForschungsZentrum Potsdam

Meyer, U., Boedecker, G., Pflug, H., 2003: Airborne Navigation and Gravimetry Ensemble & Laboratory (ANGEL), Introduction and First Airborne Tests, Scientific Technical Report STR03/06, GFZ Potsdam

Morgan, J. V., Warner, M. and the Chicxulub Working Group, 1997: Size and morphology of the Chicxulub crater, Nature, Vol. 390, 472-476

Morgan, J. V., Christeson, G. L., Zelt, C. A., 2002: Testing the resolution of a 3D velocity tomogram across the Chicxulub crater, Tectonophysics, 355, 215-226

Ness, G. E., Dauphin, J. P., Garcia-Abdeslem, J., Alvarado-Omana, M. E., 1991: Bathymetry and Gravity and Magnetics Anomalies of the Yucatán Peninsula and Adjacent Areas, Geological Society of America Map and Chart Series MCH073

Pilkington, M., Hildebrand, A. R., 2000: Three-dimensional magnetic modeling of the Chicxulub Crater, JGR, Vol. 105, No. B10, 23479-23491

Pope, K. O., Ocampo, A. C., Kinsland, G. L., Smith, R., 1996: Surface expression of the Chicxulub crater, Geology, Vol. 24, No. 6, 527-530

Rebolledo-Vieyra, M., Urrutia-Fucugauchi, J., Lopez-Loera, H., Delgado-Rodriguez, O.: Aeromagnetic anomaly modelin of the central sector of the Chicxulub impact structure, Geophys. Res. Abstr., Vol. 5, 1356, 2003

Smith, W. H. F. and Wessel, P., 1990: Gridding with continuous curvature splines in tension, Geophysics, Vol. 55, 293-305

Schwintzer, P., Reigber, C., Stubenvoll, R., Schmidt, R., Flechtner, F., Foerste, C., Bathlemes, F., Biancale, R., Balmino, G., Lemoine, J.M., 2004: A high resolution global gravity field model combining CHAMP/GRACE satellite mission and altimetry/gravimetry surface gravity data, geophysical Research Abstracts, Volume 6, EGU General Assembly, Nice, France

Urrutia-Fucugauchi, J., Marin, L., Sharpton, V. L., 1994: Reverse polarity magnetized melt rocks from the Cretacious / Tertiary structure, Yucatan peninsula, Mexico, Tectonophysics, 237, 105-112

Valliant, H. D., 1992: LaCoste & Romberg Air/Sea Meters: An Overview, CRC Handbook of Geophysical Exploration at Sea, 2nd Edition, Hydrocarbons, CRC Press

Wessel, P. and Smith, W. H. F., 1991: Free software helps map and display data, EOS Trans. Amer. Geophys. U., Vol. 72, 441, 445-446

Xu, G., Schwintzer, P., Reigber, C., 1998: KSG-Soft (Kinematic/Static GPS Software), Scientific Technical Report STR98/19, GeoForschungsZentrum Potsdam